Significance of signal recognition particle 9 nuclear translocation: Implications for pancreatic cancer prognosis and functionality

HIROMICHI SATO[1-3*], SIKUN MENG[1*], KAZUKI SASAKI[2,3], SHOGO KOBAYASHI[2,3], KANSUKE KIDO[4,5], YOSHIKO TSUJI[1], YASUKO ARAO[1], YOSHIKO SAITO[1], YOSHIFUMI IWAGAMI[2,3], DAISAKU YAMADA[2,3], YOSHITO TOMIMARU[2,3], TAKEHIRO NODA[2,3], HIDENORI TAKAHASHI[2,3], DAISUKE MOTOOKA[6], SHIZUKA UCHIDA[7], KEN OFUSA[1,8], TAROH SATOH[2,3], YUICHIRO DOKI[2,3], HIDETOSHI EGUCHI[2,3], TOMOAKI HARA[1] and HIDESHI ISHII[1]

[1]Department of Medical Data Science, Center of Medical Innovation and Translational Research, Osaka University Graduate School of Medicine, Osaka 565-0871, Japan; [2]Department of Gastroenterological Surgery, Osaka University Graduate School of Medicine, Osaka 565-0871, Japan; [3]Department of Gastroenterological Surgery, Osaka University Hospital, Osaka 565-0871, Japan; [4]Department of Pathology, Osaka University Graduate School of Medicine, Osaka 565-0871, Japan; [5]Department of Pathology, Osaka University Hospital, Osaka 565-0871, Japan; [6]Genome Information Research Center, Research Institute for Microbial Diseases, Osaka University, Osaka 565-0871, Japan; [7]Center for RNA Medicine, Department of Clinical Medicine, Aalborg University, DK-2450 Copenhagen, Denmark; [8]Prophoenix Division, Food and Life-Science Laboratory, IDEA Consultants, Inc., Osaka 559-8519, Japan

Received October 21, 2023; Accepted February 28, 2024

DOI: 10.3892/ijo.2024.5662

Abstract. Signal recognition particles (SRPs) are essential for regulating intracellular protein transport and secretion. Patients with tumors with high SRP9 expression tend to have a poorer overall survival. However, to the best of our knowledge, no reports have described the relationship between SRP9 localization and prognosis in pancreatic cancer. Thus, the present study aimed to investigate this relationship. Immunohistochemical staining for SRP9 using excised specimens from pancreatic cancer surgery cases without preoperative chemotherapy or radiotherapy showed that SRP9 was preferentially expressed in the nucleus of the cancerous regions in some cases, which was hardly detected in other cases, indicating that SRP9 was transported to the nucleus in the former cases. To compare the prognosis of patients with SRP9 nuclear translocation, patients were divided into two groups: Those with a nuclear translocation rate of >50% and those with a nuclear translocation rate of ≤50%. The nuclear translocation rate of >50% group had a significantly better recurrence-free survival than the nuclear translocation rate of ≤50% group (P=0.037). Subsequent *in vitro* experiments were conducted; notably, the nuclear translocation rate of SRP9 was reduced under amino acid-deficient conditions, suggesting that multiple factors are involved in this phenomenon. To further study the function of SRP9 nuclear translocation, *in vitro* experiments were performed by introducing SRP9 splicing variants (v1 and v2) and their deletion mutants lacking C-terminal regions into MiaPaCa pancreatic cancer cells. The results demonstrated that both splicing variants showed nuclear translocation regardless of the C-terminal deletions, suggesting the role of the N-terminal regions. Given that SRP9 is an RNA-binding protein, the study of RNA immunoprecipitation revealed that signaling pathways involved in cancer progression and protein translation were downregulated in nuclear-translocated v1 and v2. Undoubtedly, further studies of the nuclear translocation of SRP9 will open an avenue to optimize the precise evaluation and therapeutic control of pancreatic cancer.

Correspondence to: Professor Hideshi Ishii or Dr Tomoaki Hara, Department of Medical Data Science, Center of Medical Innovation and Translational Research, Osaka University Graduate School of Medicine, Yamadaoka 2-2, Suita, Osaka 565-0871, Japan
E-mail: hishii@gesurg.med.osaka-u.ac.jp
E-mail: thara@cfs.med.osaka-u.ac.jp

*Contributed equally

Key words: signal recognition particle 9, pancreatic cancer, nuclear translocation, essential amino acids, splicing variants

Introduction

Signal recognition particles (SRPs) are essential for regulating protein transport and secretion within cells (1). According to the Human Protein Atlas database (https://www.proteinatlas.org), patients with pancreatic cancer with high SRP9 expression tend to have poorer overall survival (OS). Several studies have reported the significance of SRP9 expression in several tumors, such as breast and colorectal cancer (2,3). SRP9 is highly expressed in breast (2) and colorectal (3) cancer and is considered to play a role in tumor proliferative function in colorectal cancer (4). In addition to being cancer-related, SRP9 is a febrile seizure susceptibility gene, suggesting that it may provide new clues for early diagnosis and treatment (5). SRP9, together with SRP14, binds to Alu-conserved repetitive

sequences in RNA, plays a role in the translational regulation of gene expression and metabolism of Alu transcripts (6), and combines with 40S ribosomal subunits to form stress granules (7). When binding to RN7SL1, a non-coding RNA, SRP9 inhibits the release of the RNA sensor, retinoic acid-inducible gene 1 protein (RIG-I), suppressing tumor growth (8). However, the localization of SRP9 in the tumor microenvironment remains unclear.

As summarized in previous reports, the GeneCards database (https://www.genecards.org) indicates that SRP9 is dominantly localized in the cytoplasm. However, the relationship between its localization and tumor prognosis has not, to the best of our knowledge, been elucidated. Therefore, the present study aimed to investigate the relationship between the nuclear translocation of SRP9 and patient prognosis.

Given that tumors have long been known to be stunted in methionine-deficient environments, a phenomenon known as the 'Hoffman effect' (9-13), the present study investigated whether nutrient conditions surrounding cancer cells may affect the biological behaviors of SRP9. The nuclear translocation rate of SRP9 was also examined in pancreatic cancer cells cultured in not only methionine-deficient but also tryptophan/niacin-deficient environments, which are located upstream of the methionine cycle and appear to exert a critical function in the 'Hoffman effect' (14). Furthermore, the present study examined the splicing variants of SRP9 (v1 and v2) and their deletion mutants (deletion of C-terminal regions) by molecular cloning techniques, where the genes were introduced into MiaPaCa pancreatic cancer cells, and investigated whether they were translocated to the nucleus to determine which part of the SRP9 gene contained the coding region important for nuclear translocation. Additionally, RNA immunoprecipitation (RIP) sequencing was performed on cells where v1 and v2 migrated to the nucleus, and the function of v1 and v2 was evaluated. Therefore, the present study contributed to the early detection and establishment of new treatment methods, not only for the precise evaluation and therapeutic control of pancreatic cancer, but also for other carcinomas.

Materials and methods

Patient eligibility and antibodies used for immunohistochemistry/immunocytochemistry and SRP9 variants. A total of 38 patients with pancreatic cancer who underwent surgical resection without preoperative chemotherapy or radiotherapy at Osaka University Hospital (Osaka, Japan) from December 2011 to February 2019 were included in the present study. Cases in which specimens could not be submitted because the cancer was unresectable during the surgery were excluded. The median [range] patient age was 70 [50-87] years. Resected pancreatic cancer tissues and adjacent normal tissues were obtained. Immunohistochemistry was performed on the tissues, and OS and recurrence-free survival (RFS) were examined using log rank tests depending on whether SRP9 stained ≤50% or >50% of the total number of nuclei.

Tissues were paraffin-embedded in a 10% formalin solution and stored at -20˚C postoperatively. Sections were a thickness of 20 μm. Immunohistochemistry using antibodies against SRP9 (cat. no. 11195-1-AP; RRID: AB_2239820; Proteintech Group, Inc.) (Fig. 1A and B) and Ki-67 (cat. no. 27309-1-AP; Proteintech Group, Inc.) (Fig. S1A) were performed using the excised specimens at concentrations of 1:200, and 1:2,500, respectively, and both were incubated at 4˚C for 24 h. Normal goat serum blocking solution (cat. no. S-1000-20; Vector Laboratories, Inc.; Maravai Life Sciences) was used at a concentration of 1:200 for 60 min at room temperature for blocking, and anti-IgG (H+L), rabbit, goat-polyclonal secondary antibody (cat. no. BA-1000-1.5; Vector Laboratories Inc.; Maravai Life Sciences) was used at a concentration of 1:500 for 60 min at room temperature. Antigen activation was performed by heating at 100˚C for 40 min in Antigen retrieval buffer (1 l of distilled water mixed with 1.92 g of anhydrous citric acid to reach pH 6), and phosphate buffered saline (PBS) was used as the washing reagent. Rehydration in an alcohol series was performed with gradually increasing concentrations of 60, 70, 80, 90, 95 and 100% ethanol. VECTASTAIN® Elite® ABC-HRP Kit, Peroxidase (cat. no. PK-6100; Vector Laboratories Inc.; Maravai Life Sciences) was used for primary/secondary antibody binding, followed by visualization with a DAB Tablet (cat. no. 045-22833; Vector Laboratories Inc.; Maravai Life Sciences). For color development, the specimen was incubated with 3,3'-diaminobenzidine for 60 sec. Specimens with immunohistochemical staining were observed using an all-in-one fluorescence microscope (BZ-X710; Keyence Corporation). Subsequently, the relationship between nuclear staining rate and Ki-67 was examined using single regression analysis. The rate of nuclear staining and Ki-67 was evaluated by an expert pathologist.

This study was approved by the Research Ethics Committee of Osaka University (approval number. 23158). Written informed consent for participation was obtained from all subjects involved in the study and for publication.

Cell lines and culture conditions. The cell culture dish used was a VTC-D100, ϕ93x20 mm in size (cat. no. 2-8590-03; Violamo). Within the present study, all medium used was maintained at 37˚C with 5% CO_2, and medium was replaced every other day with 10 ml medium. During cell passages, the cells were washed with 5 ml Dulbecco's phosphate-buffered saline (D-PBS; cat. no. 14249-24; Nacalai Tesque, Inc.) and incubated with 3 ml trypsin (cat. no. 12605010; Thermo Fisher Scientific, Inc.) for 3 min at 37˚C, then centrifuged (4˚C, 120 x g, 4 min). After the supernatant was removed, the cells were resuspended with the original medium and seeded into a new dish at the desired density with 10 ml medium.

The cell lines we used in the present study were MiaPaCa [human pancreatic cancer (ATCC® CRL-1420™)], Panc10.05 [human pancreatic cancer (ATCC® CRL-2547™)], Caski [human cervical cancer (ATCC® CRL-1550™)], 293T [human fetal renal cells (ATCC® CRL-3216™)] and HT-29 [human colon cancer cells (ATCC® HTB-38™)] cells. The cell lines were utilized at early passages after being obtained from the cell bank (ATCC) and examined for negative mycoplasma infections before the *in vivo* experiment by the Central Institute for Experimental Animals, Japan (https://www.ciea.or.jp/about/).

Immunocytochemistry to evaluate differences in nuclear translocation rates between pancreatic cancer lines cultured in normal and amino acid-deficient media. The following *in vitro* experiments were conducted to investigate the

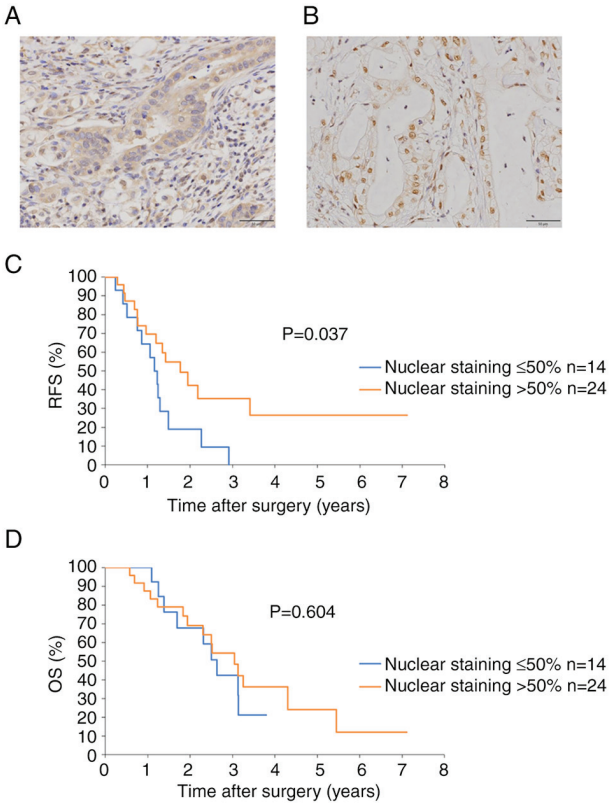

Figure 1. Comparison of patient prognoses (RFS and OS) in two SRP9 expression groups. In immunohistochemistry staining for SRP9, the tumors were divided into two groups: (A) Staining of ≤50% of the total number of nuclei in the tumor and (B) staining of >50% of the tumor area (magnification, x40; scale bar, 50 μm). The (C) RFS and (D) OS of the two SRP9 expression groups were compared. RFS, recurrence-free survival; OS, overall survival; SRP9, signal recognition particle 9.

relationship between differences in nuclear translocation rates and amino acid availability. The deficient nutrients were the essential amino acid, methionine, plus niacin/tryptophan, which is located in its upstream mechanism of the methionine cycle (Fig. 2A).

The pancreatic cancer cell line, MiaPaCa, cultured in Dulbecco's Modified Eagle's Medium with amino acids (cat. no. 08456-36; Nacalai Tesque, Inc.) and 10% fetal bovine serum (FBS) (hereinafter referred to as 'regular medium') for 24 h was divided and cultured in four types of media: i) Medium containing methionine, tryptophan and niacin [hereinafter referred to as 'MTN(+)'], consisting of L-amino acids (arginine, cysteine, glutamine, histidine, isoleucine, leucine, lysine, methionine, phenylalanine, threonine, tryptophan, tyrosine and valine), niacin [despite not strictly being an amino acid, it is located upstream of the methionine cycle with tryptophan (Fig. 2A)], amino-free Dulbecco's Modified Eagle's Medium (cat. no. 20780-25; specially prepared reagent, DMEM (Low Glucose) with Sodium Pyruvate, without Amino Acids and Nicotinamide; Nacalai Tesque, Inc.) and 10% dialyzed FBS (SH30079.03; Cytiva); ii) methionine-free medium [hereinafter referred to as 'M(-)']; iii) tryptophan- and niacin-free medium [hereinafter referred to as 'TN(-)']; and iv) methionine-, tryptophan- and niacin-free medium [hereinafter referred to as 'MTN(-)']. After 24 h of incubation, cells were fixed with 4% paraformaldehyde for 15 min at room temperature and were permeabilized with a solution containing 0.1% Triton X-100 and 1% bovine serum albumin (cat. no. A7906; Sigma-Aldrich; Merck KGaA) in PBS for 30 min at room temperature. Blocking was performed using a solution composed of Blocking One Histo (cat. no. 06349-64; Nacalai Tesque, Inc.), diluted in PBS with 0.1% Tween-20, for 30 min at room temperature. Immunocytochemistry of SRP9 and the nuclei was performed using the same SRP9 primary antibody as aforementioned. The Goat anti-Rabbit IgG (H+L) Cross-Adsorbed Secondary Antibody, Alexa Fluor™ 594 (1:200: cat. no. A-11012; Invitrogen; Thermo Fisher Scientific, Inc.) was then incubated with the sample for 30 min at room temperature in the dark. The cell nuclei were stained with DAPI (Dojindo Laboratories, Inc.). The treated cells were then observed under an all-in-one fluorescence microscope (BZ-X710; Keyence Corporation). Image analysis was performed using the Analysis Application Hybrid cell count software (BZ-H3C; Keyence Corporation).

After confirming that SRP9 and DAPI fluorescence was observed in all four conditions, MTN(+) (Fig. S2A), M(-) (Fig. S2B), TN(-) (Fig. S2C) and MTN(-) (Fig. S2D), the nuclear translocation rate was determined as follows. The area of SRP9 staining [S_{all}, area defined as 'Cytoplasm and nucleus stained with SRP9' (Fig. 2B)] and the area where SRP and DAPI staining overlapped [S_{nuclei}, area defined as 'Overlap area' (Fig. 2B)] were measured. In one sample, 16 locations were randomly selected (Fig. 2C), and for each, an image with SRP9 fluorescence (Fig. 2D) and an image with DAPI overlap (Fig. 2E) were collected to determine the nuclear translocation rate, which is represented by the formula 'S' (nuclear translocation rate=S_{nuclei}/S_{all}). The ratio of the area of SRP9 staining multiplied by the fluorescence intensity was also taken to define the nuclear transfer rate as 'R' (nuclear translocation rate=R_{nuclei}/R_{all}). R=S x fluorescence intensity.

Evaluation of SRP9 variants in different nutrient conditions and the nuclear translocation of artificially constructed SRP9 isoforms. A total of two variants of SRP9 are known to exist, variant 1 (v1) and variant 2 (v2) (https://www.ncbi.nlm.nih.gov/gene/6726) (Fig. 3A). v1 contains exons 1, 2 and 3 in the coding region, and v2 contains exons 1, 2 and 4 in the coding region.

MiaPaCa cells were cultured in regular medium for 24 h and then cultured in M(-), TN(-), MTN(-) or MTN(+) for 24 h. Total RNA extraction was performed using ISOGEN (Nippon Gene Co., Ltd.), and reverse transcription was performed using PrimeScript RT Master Mix (Takara Bio USA, Inc.) according to the manufacturer's instructions. In this process, proteins were removed by phenol-associated extraction. Polymerase chain reaction (PCR) was then performed using PrimeSTAR Max DNA Polymerase (Takara Bio USA, Inc.) according to the manufacturer's instructions. Electrophoresis was performed using a 0.9% agarose gel at a voltage of 100 V, with Midori Green Direct (cat. no. MG06; NIPPON Genetics EUROPE GmbH) used as the fluorescent dye for visualization. Images were acquired using a ChemiDoc multiplex fluorescence imaging system (ChemiDoc MP; Bio-Rad Laboratories, Inc.), and the results were quantified using Image Lab software v6.1 (Bio-Rad Laboratories, Inc.). v1 (500 bp) and v2 (274 bp) of SRP9 were amplified using the same forward and

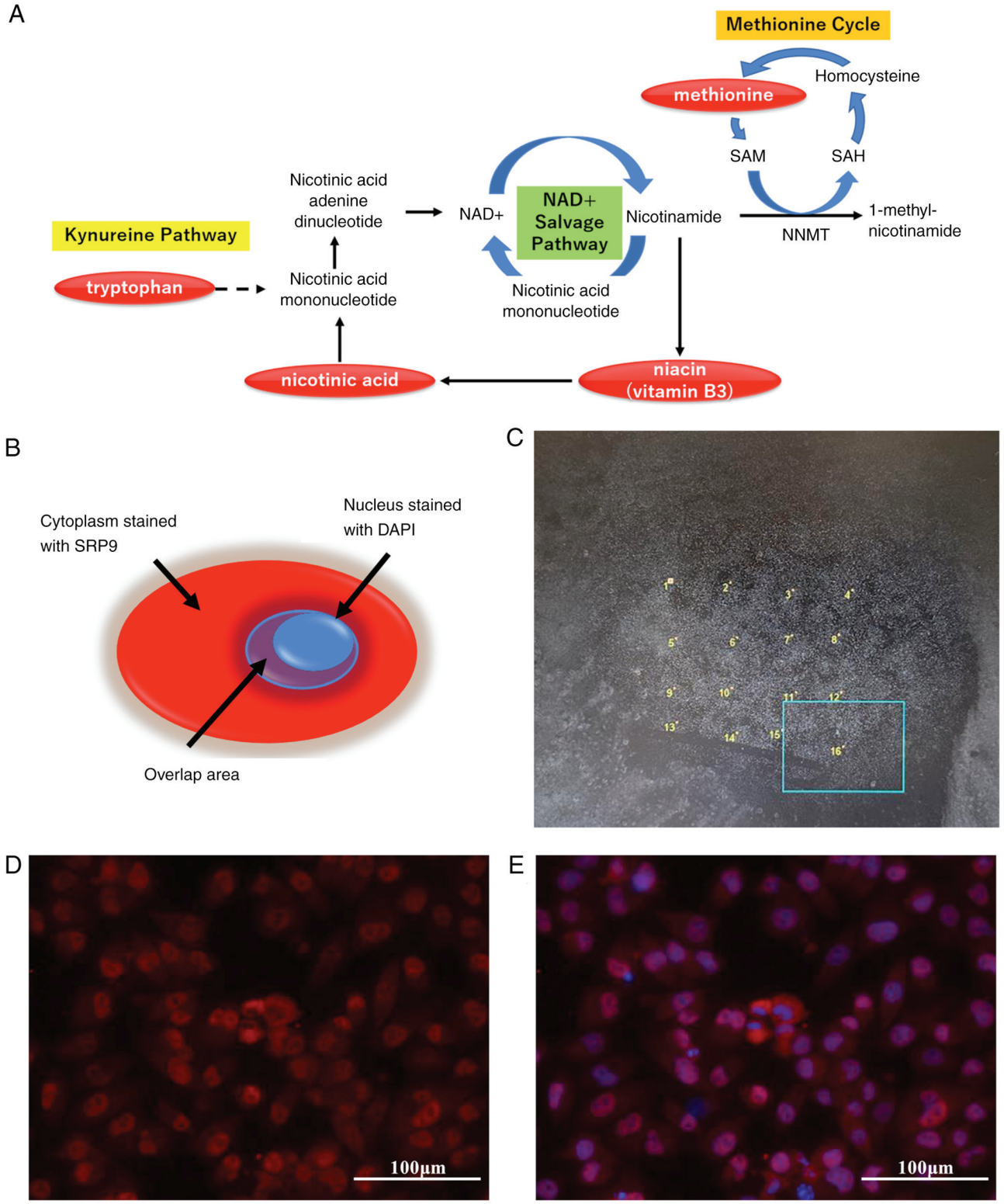

Figure 2. Continued.

reverse primers: Forward, 5'-CACTCTAGGCCACGATGCCG-3' and reverse, 5'-CACTCAGTTTCCATGGTAAC-3' (Fig. S3A and B). PCR and electrophoresis were also performed under the same conditions for GAPDH as the housekeeping gene (Fig. S3C), using the following primers: Forward 5'-TGGTATCGTGGAAGGACTCATG-3' and reverse, 5'-AGAGGCAGGGATGATGTTCTG-3'.

Then, the following experiment was performed to determine the nuclear localization signal of SRP9 (Fig. 3B). After culturing MiaPaCa cells in regular medium for 24 h, a portion of the cells were observed under an all-in-one fluorescence microscope as the negative control MOCK cells (Fig. 3C). The cells were then transfected with plasmids consisting of the pDsRed2-N1 vector and artificial genes of v1 or v2 or

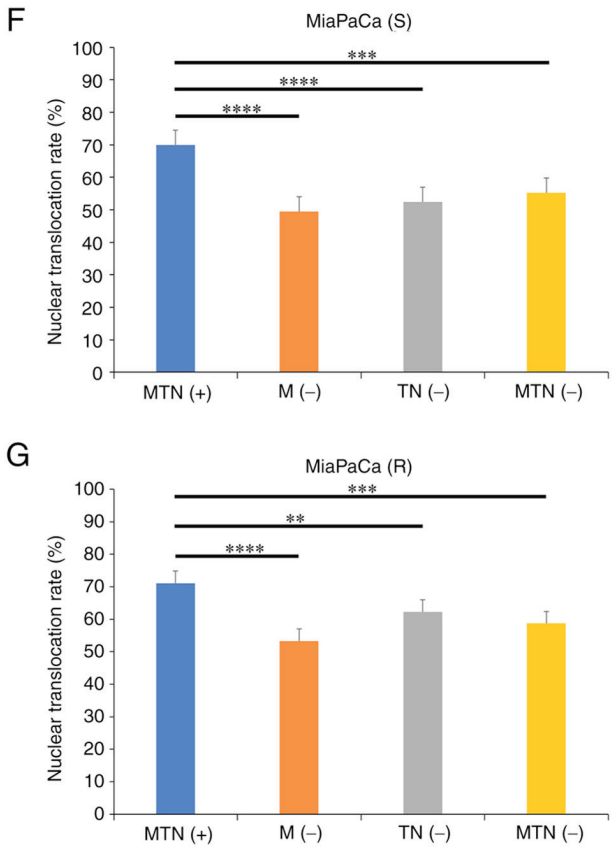

Figure 2. Immunocytochemistry to evaluate differences in nuclear translocation rates between pancreatic cancer lines cultured in normal and amino acid-deficient medium. (A) The pathway of methionine and tryptophan/niacin upstream of the cycle, which is deficient in the medium used in the present study. (B) The 'Cytoplasm stained with SRP9' and the 'Overlap area,' which are the staining covers of DAPI and SRP9 used in the 'S' and 'R' equations. The MiaPaCa pancreatic cancer cell line was cultured in regular medium for 24 h and then divided into four different media: MTN(+), M(-), TN(-) and MTN(-). After 24 h of incubation, SRP9 and nuclear immunocytochemistry tests were performed. (C) A total of 16 locations were randomly selected in one sample. The area of SRP9 (S_{all}, defined as 'cytoplasm stained with SRP9') and the area where SRP9 and DAPI overlapped (S_{nuclei}, defined as 'overlapping area') were measured to determine S (nuclear transfer rate=S_{nuclei}/S_{all}), and the nuclear translocation rate expressed by the equation S was calculated. The nuclear transfer rate was defined as R [nuclear transfer rate=R_{nuclei}/R_{all} (R=S x fluorescence intensity)] by taking the ratio of the area of SRP9 multiplied by the fluorescence intensity. Representative images with (D) SRP9 fluorescence and (E) DAPI overlap. MiaPaCa cells were cultured in MTN(+), M(-), TN(-) or MTN(-), and the nuclear transfer rates were compared using the equations expressed as (F) S and (G) R. Error bars indicate standard error. **P<0.01, ***P<0.001, ****P<0.0001 by Dunn test. Images of immunocyte staining were collected at x40 magnification, and the scale bars indicate 100 μm. SAM, S-adenosylmethionine; SAH, S-adenosylhomocysteine; NNMT, nicotinamide N-methyltransferase; NAD^+, nicotinamide adenine dinucleotide; SRP9, signal recognition particle 9; MTN(+), consisting of L-amino acids, niacin and tryptophan; M(-), methionine-free medium; TN(-), tryptophan- and niacin-free medium; MTN(-), methionine-, tryptophan- and niacin-free medium.

the common part of v1 and v2 (containing exons 1 and 2). After culturing for 48 h, the cell nuclei were stained with Hoechst 33342 nucleic acid stain (Invitrogen; Thermo Fisher Scientific, Inc.) and observed under an all-in-one fluorescence microscope.

The inserts for v1 or v2 or the common part of v1 and v2 were purchased from Eurofins Genomics K.K. The pDsRed2-N1 vector, which expresses DsRed2 red fluorescent protein, is kanamycin-resistant and was purchased from Takara Bio USA, Inc. Plasmid digestion of the inserts and vector was performed using the restriction enzymes *Xho*I (on the 5' side) and *Bam*HI (on the 3' side) (Takara Bio Inc.). Ligation was then conducted using T4 DNA ligase (Takara Bio Inc.). Lipofectamine 3000 Transfection Reagent (Invitrogen; Thermo Fisher Scientific, Inc.) was used for transfection with 500 ng of nucleic acid. The transfection was performed at 37˚C with 5% CO_2 for 48 h. Following transfection, cell nuclei were stained with Hoechst 33342 (cat. no. H1399; Invitrogen; Thermo Fisher Scientific, Inc.) and observed using the all-in-one fluorescence microscope.

Functional evaluation of v1 and v2 by RIP sequencing. An overview of the RIP sequencing protocol is shown in Fig. 4A. A total of $1x10^7$ MiaPaCa pancreatic cancer cells were cultured in a 15-cm plastic culture dish (Nunc; Thermo Fisher Scientific, Inc.) in RPMI1640 (Nacalai Tesque, Inc.) with 10% FBS under 5% CO_2 at 37˚C. The MiaPaCa cell lines before transfection of v1 (Fig. 4B) or v2 (Fig. 4C) plasmids were observed as MOCK cells using a fluorescent all-in-one microscope, and no AcGFP signal was observed in both cases. SRP9V1-3xFLAG and SRP9V2-3xFLAG genes were prepared by DNA synthesis (Eurofins Genomics K.K.), the sequences of which were confirmed by Sanger sequencer (ABI GmbH). pIRES2-AcGFP1-NLS-SRP9V1-3xFLAG and pIRES2-AcGFP1-NLS-SRP9V2-3xFLAG vectors were designed to express exogenous SRP9V1-3xFLAG or SRP9V2-3xFLAG genes in the split protein by the internal ribosome entry site signal, an RNA element enabling cap-independent initiation of translation as part of the process of protein synthesis, from AcGFP1 under NLS, which is fused with exogenous SRP9V1-3xFLAG or SRP9V2-3xFLAG. The SRP9V1 or SRP9V2 peptide was translated in-frame with a 3xFLAG peptide (MDYKDHDGDYKDHDIDYKDDDDK). Transfection of pIRES2-AcGFP1-NSL-SRP9V1 or pIRES2-AcGFP1-NSL-SRP9V2 plasmids was performed by electroporation using a Nepa Gene Co., Ltd. system, which allows for the preservation of membrane damage during transfection compared with Lipofectamine methods. The cells were cultured in RPMI1640 with 10% FBS and 200 mg/ml geneticin (Nacalai Tesque, Inc.) for 2 weeks to select gene-transfected cells. Protein expression was then confirmed by the presence of AcGFP signal using a fluorescent all-in-one microscope for both v1 (Fig. 4D) and v2 (Fig. 4E).

A total of $5x10^6$ AcGFP expressing cells were collected by fluorescence-activated cell sorting (BD Biosciences), cultured in RPMI1640 with 10% FBS for 24 h and subjected to protein extraction. For protein extraction, adherent cells were washed with PBS(-) (Nacalai Tesque, Inc.) three times in a 15-cm plastic culture dish to exclude amino acids in the medium that can interfere with the cross-linker. The cells were harvested with plastic cell scrapers and collected in 2 ml tubes. Samples were then centrifuged at 280 x g at 4˚C for 5 min, and the collected cell pellets were lysed in 1 ml HEPES-RIPA [150 mM KCl, 50 mM HEPES-NaOH (pH7 4), 1% NP-40 and 1X Roche cOmplete proteinase inhibitor, prepared from 50X stock reagent (cat. no. 04693116001; Roche Diagnostics)]. Samples were centrifuged again at 280 x g at 4˚C for 5 min, and the collected cell lysates were incubated

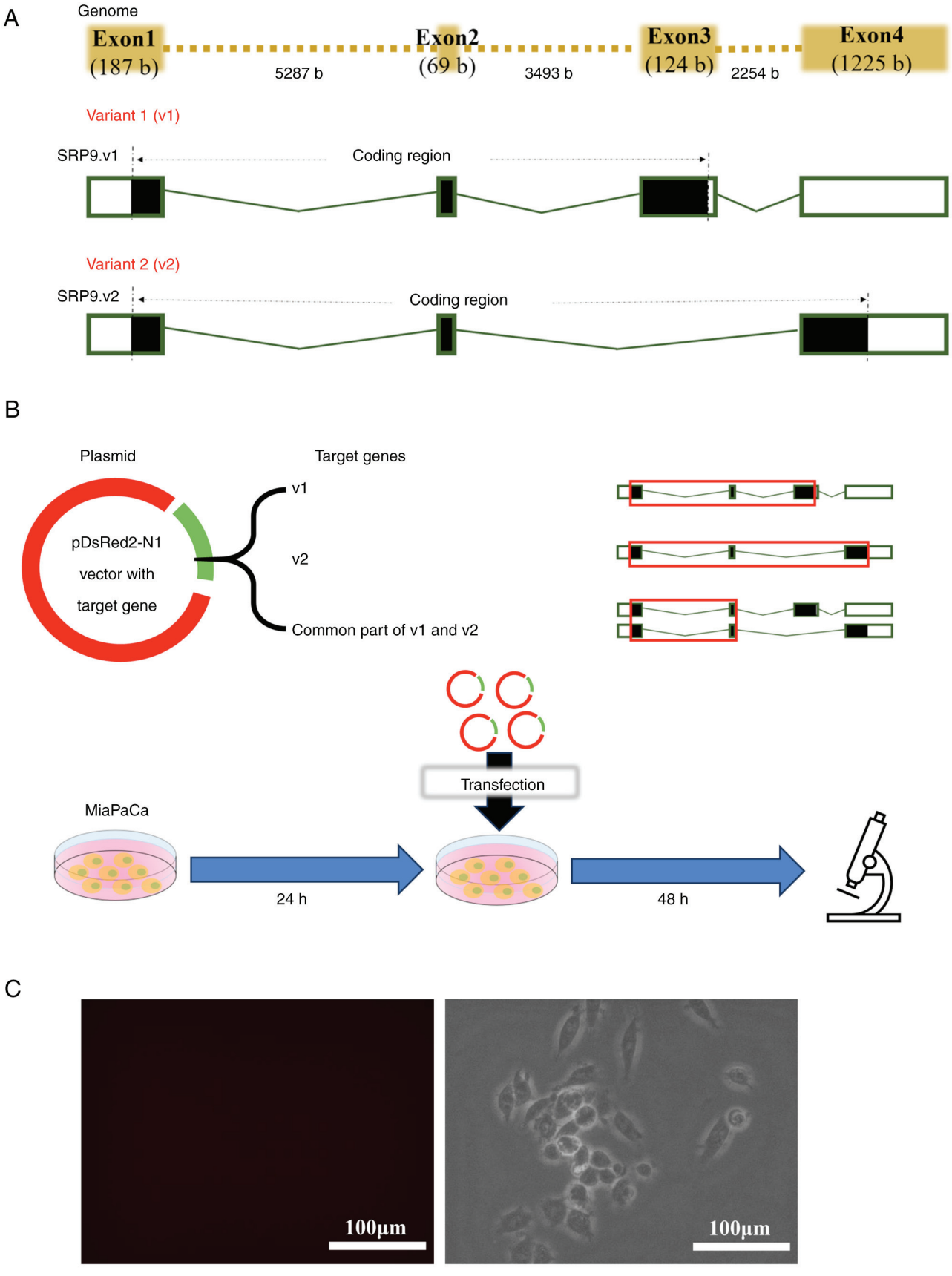

Figure 3. Continued.

for 30 min at room temperature with the cross-linking agent, bis(sulfosuccinimidyl)suberate (Thermo Fisher Scientific, Inc.), which does not permeate cell membranes. Therefore, permeabilization was conducted with the treatment of the

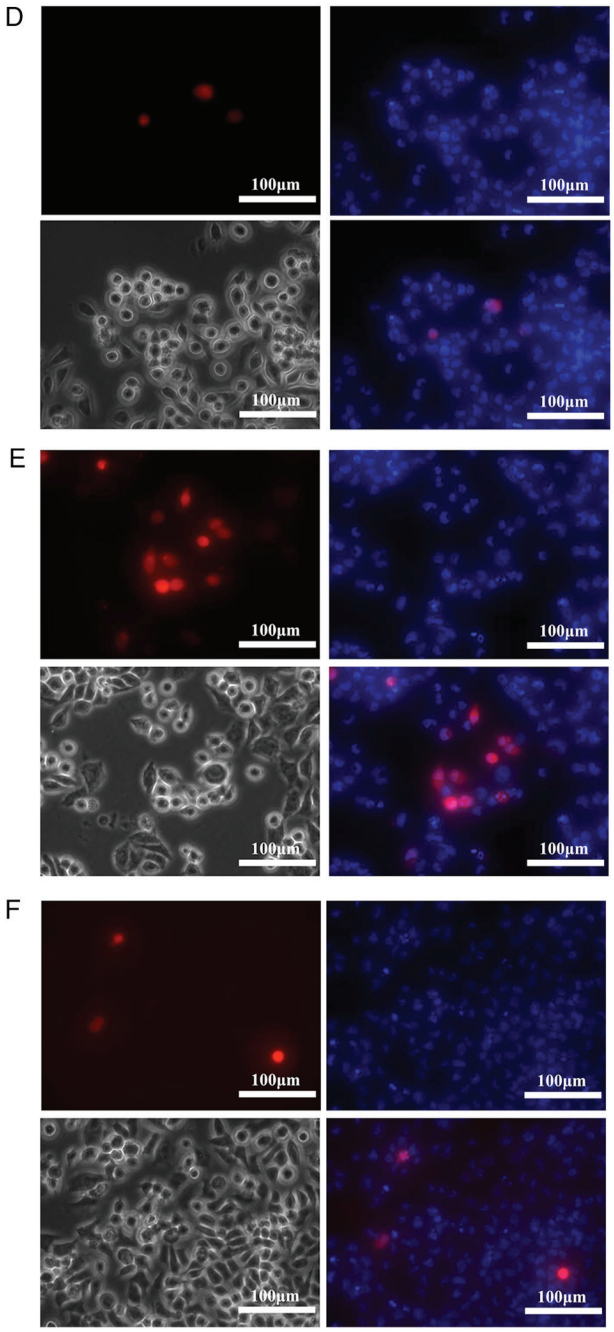

Figure 3. Evaluation of nuclear translocation of artificially constructed SRP9 isoforms. (A) Variants of SRP9, v1 and v2. (B) MiaPaCa cells cultured in regular medium for 24 h were transfected with plasmids incorporating the genes of v1, v2 and the common parts of v1 and v2 and cultured for 48 h, after which fluorescence was observed under a microscope. (C) SRP9 expression was not observed in MOCK cells prior to transfection with the plasmids. The results of fluorescence in (D) v1, (E) v2, and (F) the common parts of v1 and v2. Images of immunocyte staining were collected at x40 magnification, and the scale bars indicate 100 μm. v1, variant 1; v2, variant 2; SRP9, signal recognition particle 9.

surfactant, NP-40, as aforementioned. Newly purchased bis(sulfosuccinimidyl)suberate (lot no. YB351210) was used due to its ability to absorb moisture from the atmosphere and become inactive. After the cross-linking reaction, 1/50 (final concentration, 20 mM) 1 M Tris-HCl (pH 7.5) was added to the tube to quench the excess cross-linking agent, followed by gentle mixing by inversion for 15 min. Samples

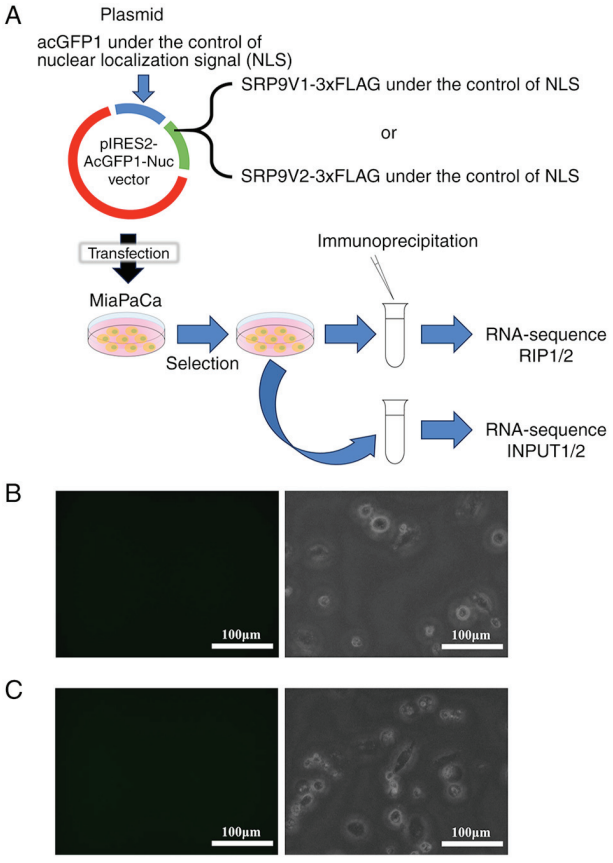

Figure 4. Continued.

were subjected to immunoprecipitation to purify the target SRP9V1-3xFLAG or SRP9V2-3xFLAG proteins. To this end, 20 μl anti-DDDDK antibody (undiluted at a concentration of 0.675 mg/ml; cat. no. ab205606; Abcam), which binds to the FLAG tag sequence, was added to each sample in 10 μl (6.75 μg of antibody), incubated at 4˚C overnight (16 h) and purified with protein A and G conjugated magnetic beads (Bio-Rad Laboratories, Inc.). The total amount of Protein A and G added was 1 mg (0.5 mg Protein A + 0.5 mg Protein G) per sample. The immunoprecipitated SRP9V1-3xFLAG or SRP9V2-3xFLAG protein cross-linked with endogenous RNA was washed with 1 ml HEPES-RIPA [150 mM KCl, 50 mM HEPES-NaOH (pH 7.4], and 1% NP-40), 1 ml high salt HEPES-RIPA [300 mM KCl, 50 mM HEPES-NaOH (pH 7.4), and 1% NP-40] and once again with 1 ml HEPES-RIPA, which were used to remove non-specific bound substances from the protein A and G conjugated magnetic beads. Finally, samples were treated with 100 mg 3X DYKDDDDK peptide (FP-1; Sigma-Aldrich; Merck KGaA) to elute endogenous RNA-bound SRP9V1-3xFLAG or SRP9V2-3xFLAG proteins (hereinafter referred to as 'RIP1' and 'RIP2,' respectively).

RNA was extracted from the samples using the RNeasy Mini Kit (cat. no. 74104; Qiagen GmbH), and 100 ng RNA was subjected to the high-speed sequencing system, NovaSeq6000 (Illumina, Inc.). Each Illumina sequencing library was prepared using SMARTer Stranded Total RNA-seq Kit v2-Pico Input Mammalian Components (cat. no. 634417; Takara Bio USA, Inc.). As controls, input RNAs from geneticin-selected transfected cells with SRP9V1-3xFLAG or SRP9V2-3xFLAG

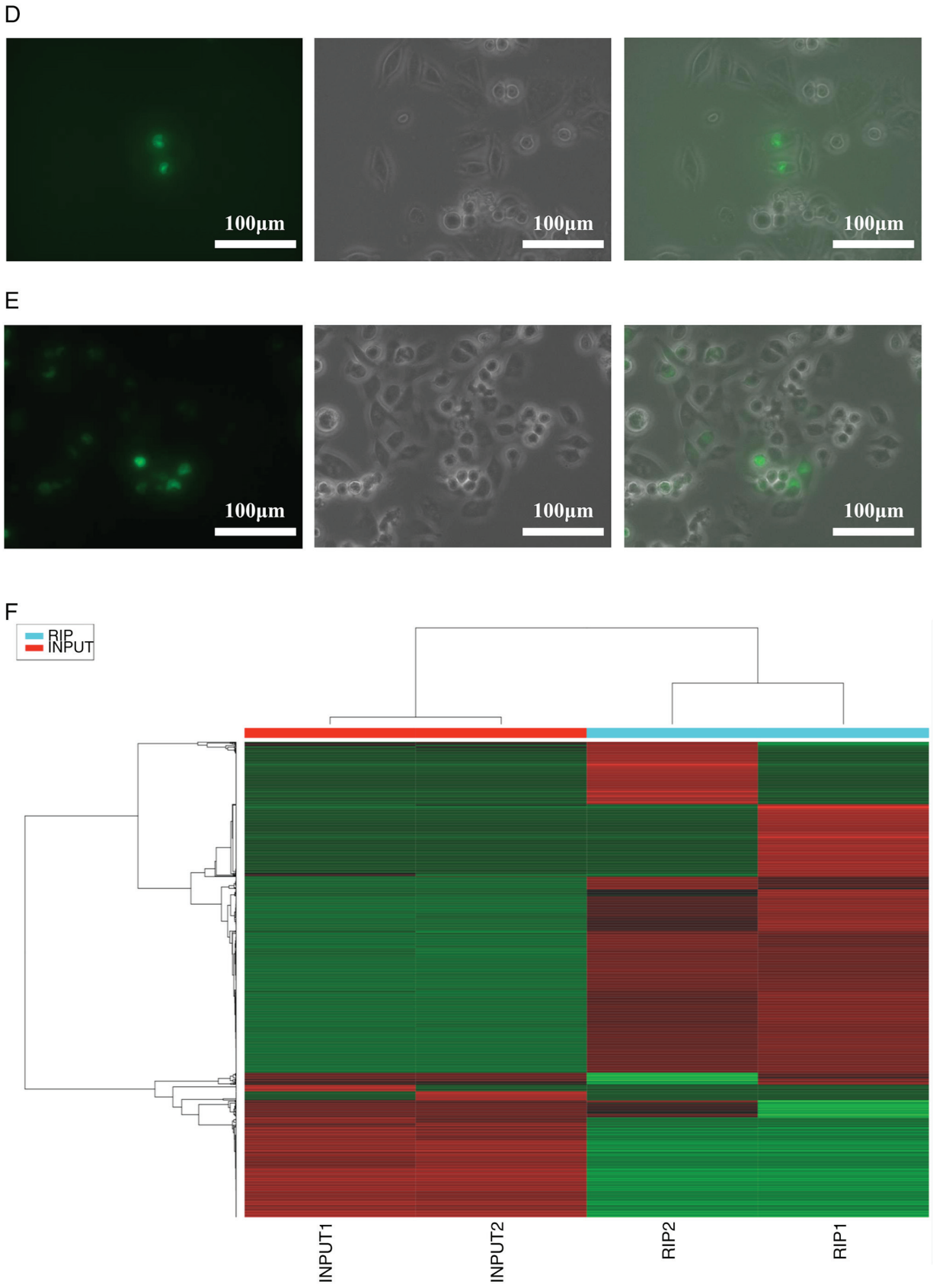

Figure 4. Continued.

(hereinafter referred to as 'INPUT1' and 'INPUT2,' respectively) (Fig. 4A) were prepared and used. To confirm the quality/completeness of the processed samples, the length distribution of the constructed libraries was inspected by LabChip GX (Perkin Elmer, Inc.), with 101 bp paired ends as the sequencing type. The sequencing kits, NovaSeq 6000 S1 Reagent Kit v1.5

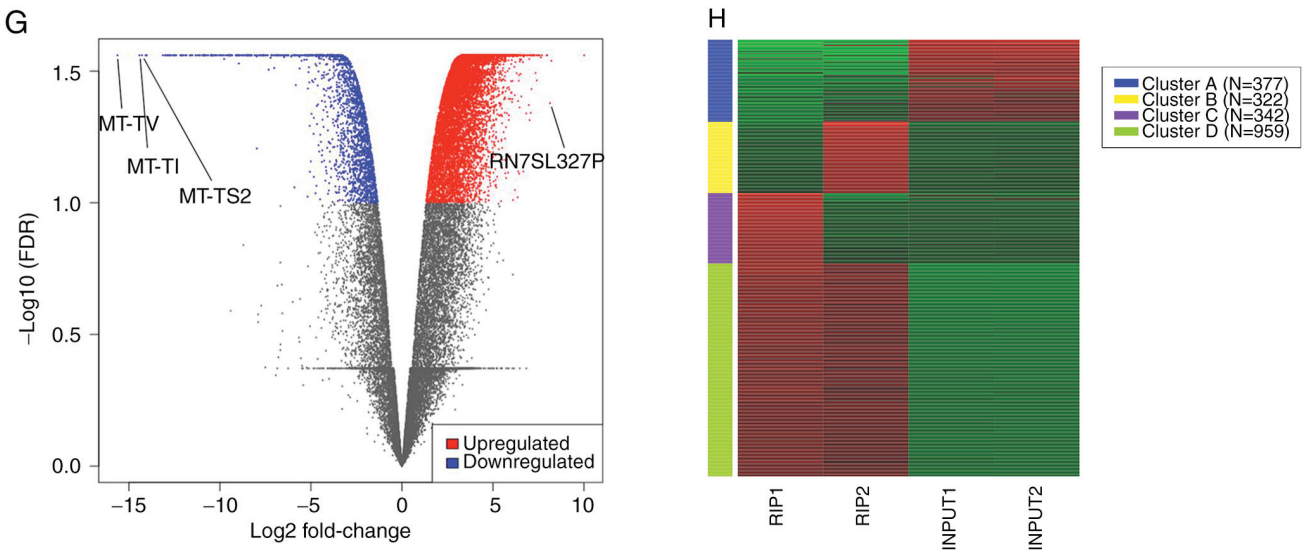

Figure 4. Continued.

(200 cycles; cat. no. 20028318; Illumina, Inc.) or NovaSeq 6000 S2 Reagent Kit v1.5 (200 cycles; cat. no. 20028315; Illumina, Inc.) were used. The loading concentration of the final library was 320 pM and concentrations were measured using KAPA Library Quantification DNA Control Standard (KAPA Biosystems; Roche Diagnostics). The sequencing was performed by the NGS core facility at the Research Institute for Microbial Diseases of Osaka University (Osaka, Japan).

The normalized fragments per kilobase million data from RIP1, RIP2, INPUT1 and INPUT2 were used to create a heatmap, volcano plot, and k-means clustering and to perform pathway and enrichment analyses using iDEP.96 (sdstate.edu). Gene set enrichment analysis (GSEA) was performed using GSEAPreranked (GSEAPreranked v4.3.2; 1,000 permutations; enrichment statistic=weighted; max size=500; min size=15; normalization mode=meandiv; ranked by t-score), based on genes that were either up- or downregulated with P<0.05, using these collections of gene sets from the Molecular Signatures Database (h.all.v2023.Hs.symbols.gmt): i) Hallmarks, ii) canonical, iii) Gene Ontology, iv) chemical and genetic perturbations, v) immunologic signatures, vi) oncogenic signatures, and vii) cancer modules. Gene sets were considered significantly enriched and met the threshold of NOM P<0.05.

In vitro tumor viability under amino acid depletion. A total of $4x10^3$/ml of each tumor cell line (Panc10.05, Caski and 293T) was divided into two groups (n=4) and cultured in regular medium for 24 h. The media of one group were then changed to MTN(+) medium (as the control), and the media of another group were changed to M(-) medium for 48 h. The MTT formazan product assay was then conducted (Fig. S4A). Dimethyl sulfoxide was used to dissolve the purple formazan, and the wavelength used for the formazan measurement was 450 nm.

Amino acid dependence of cancer in mice. All experiments were approved by the Osaka University Animal Experiments Committee, the formal ethics committee for institutional animal study at Osaka University (approval no. 30-011), and conducted in accordance with the Osaka University Regulations on Animal Experiments. Female 5-week-old wild-type NOD SCID mice, derived from a mouse strain with a naturally occurring mutant, exhibiting an autosomal recessive inheritance pattern and severe immunodeficiency due to the absence of T and B cells, which results in minimal rejection of xenogeneic cells and tissues, were procured from Japan SLC, Inc. Mice were randomly divided into cages for each feeding condition described below. Not only methionine but also its upstream pathways are involved in cancer immunity. Tryptophan/niacin located upstream of the methionine cycle is metabolized to form nicotinamide, which is related to the methionine pathway, and 1-methyl-nicotinamide (MNAM) is formed from S-adenosylmethionine (SAM) synthesized from methionine via nicotinamide N-methyltransferase. Thus, MNAM synthesized in this methionine cycle is said to suppress T cells and promote cancer (15). Therefore, the HT-29 human colon cancer cell line cultured in regular medium containing all nutrients was used to induce tumors that did not cause detectable clinical side effects. For this, $2x10^5$ cells, were transplanted subcutaneously into the back of NOD SCID mice in accordance with the Guidance on the Operation of Animals (Scientific Procedures) Act 1986. Some mice were reared for 2 weeks on a diet devoid of methionine, tryptophan and niacin. The median (range) body weight of the mice at the beginning of the experiment was 16 (13-17) g. Mice raised on a normal diet containing methionine, tryptophan and niacin were defined as MTN(+), mice raised on a methionine-free diet were defined as M(-), mice raised on a tryptophan- and niacin-free diet were defined as TN(-) and mice raised on a methionine-, tryptophan- and niacin-free diet were defined as MTN(-). Special diets for the mice were custom-ordered with as much appearance and taste as the normal diet as possible. Rearing conditions were such that the floor was changed daily to minimize the intake of excretory-derived amino acids (Fig. S5A). The room temperature was maintained at ~23˚C and the lights were turned on in 12 h cycles. Although the initial plan was to euthanize the mice if the tumor size exceeded 150 mm^3 or

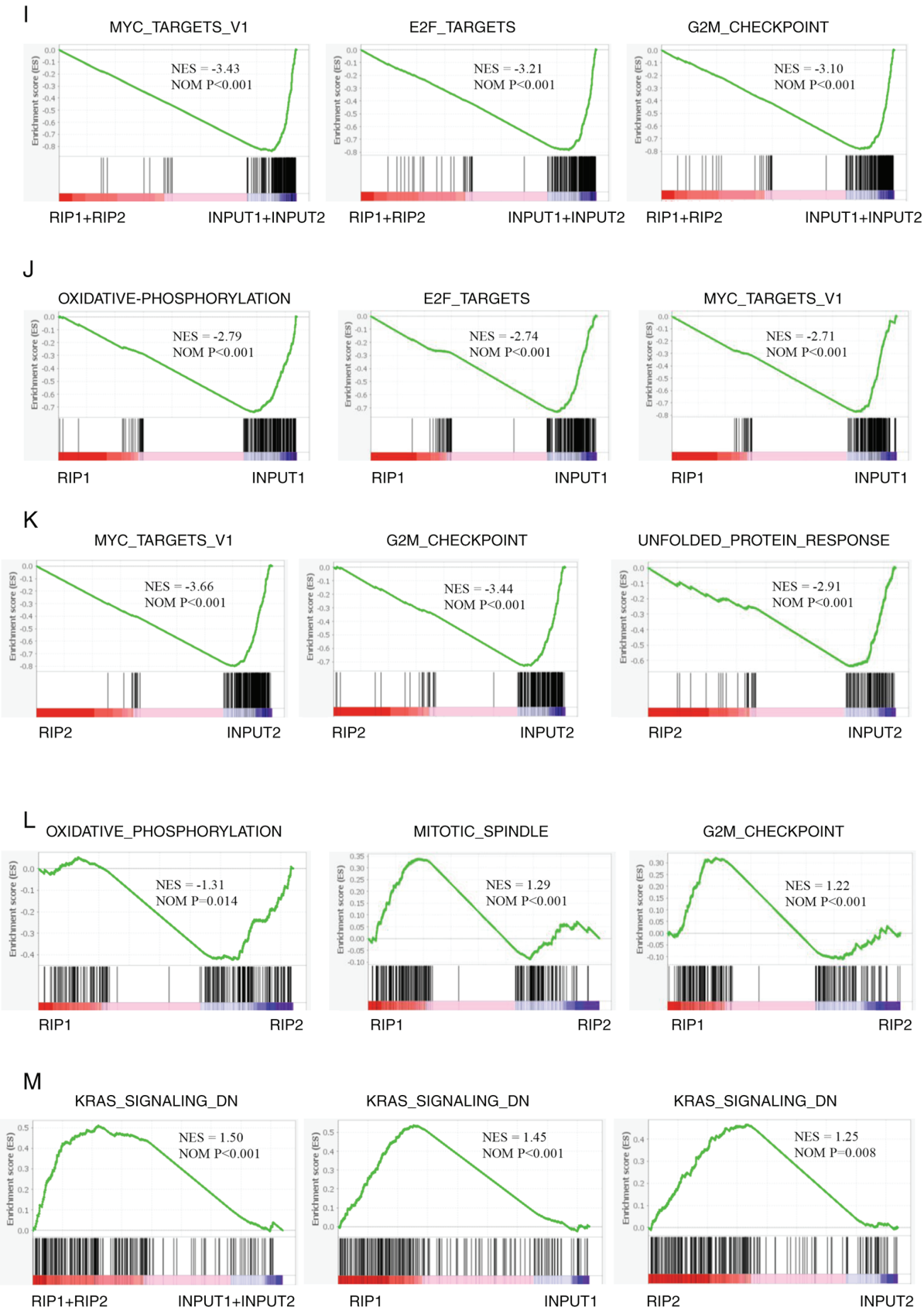

Figure 4. Functional evaluation of v1 and v2 by RIP sequencing. (A) Overview of RIP sequencing. The MiaPaCa cell line before transfection of the SRP9 (B) v1 and (C) v2 plasmids (MOCK cells) showed no AcGFP signal in both cases when observed using a fluorescent all-in-one microscope. Then, protein expression of (D) v1 and (E) v2 via AcGFP signal was confirmed following transfection with pIRES2-AcGFP1-NSL-SRP9V1 or pIRES2-AcGFP1-NSL-SRP9V2 plasmids. Results of the (F) heatmap, (G) volcano plot and (H) cluster analysis using the k-means algorithm for RIP1, RIP2, INPUT1 and INPUT2. Top pathways enriched in GSEA for (I) RIP1 + RIP2 vs. INPUT1 + INPUT2, (J) RIP1 vs. INPUT1, (K) RIP2 vs. INPUT2 and (L) RIP1 vs. RIP2. (M) In the GSEA, the KRAS signaling DN pathway was the most upregulated in the RIP samples for RIP1 + RIP2 vs. INPUT1 + INPUT2, RIP1 vs. INPUT1, and RIP2 vs. INPUT2. v1, variant 1; v2, variant 2; SRP9, signal recognition particle 9; RIP, RNA immunoprecipitation (sample); FDR, false discovery rate; GSEA, Gene Set Enrichment Analysis; DN, downregulated; NES, Normalized Enrichment Score; NOM, nominal.

if the weight of the mice increased by >20% within 1 week, the intended 3-week experimental period was successfully completed without encountering any breaches of these restrictions. Euthanasia experiments using CO_2 were conducted in accordance with the American Veterinary Medical Association (AVMA) guidelines and with ethical considerations to minimize suffering. For mice weighing ~20 g, the concentration of CO_2 used for euthanasia was 40%, with a flow rate of 0.5 l/min for an inhalation time of 10 min. For smaller mice weighing ≤16 g, the concentration of CO_2 was reduced within the range of 30-40%, with a lower flow rate of 0.2-0.5 l/min and for a shorter inhalation time of 5-10 min, to minimize stress and pain to the mice during the procedure. Mice were continuously observed during the procedure and, since the AVMA guideline recommends a 30-70% vol/min displacement rate of the euthanasia chamber, the euthanasia chamber was set at 30-40%. The experiment was first performed with 1 MTN(-) mouse as a first step (Fig. S5B), followed by a second step with an additional MTN(+) mouse with n=1, M(-) mice with n=2, TN(-) mouse with n=1 and MTN(-) mouse with n=1 (Fig. S5C).

The tumors were then removed from the mice and evaluated for RNA expression and type by RNA sequencing (Fig. S5A). After confirming the cessation of mouse respiratory movements, tumors were promptly excised within 30 min in a well-maintained environment with laboratory air conditioning and a clean experimental table. Subsequently, the tumors were immersed in RNA LATER reagent (Sigma-Aldrich; Merck KGaA), and RNA was extracted using QIAzol Lysis Reagent (cat. no. 79306; Qiagen GmbH), followed by RNA sequencing analysis. RNA libraries were prepared using a TruSeq Stranded mRNA Library Prep Kit (cat. no. 20020595; Illumina, Inc.). To confirm the quality/completeness of the processed samples, the length distribution of the constructed libraries was inspected by LabChip GX (Perkin Elmer, Inc.), with 101 bp paired ends as the sequencing type. The sequencing kits, NovaSeq 6000 S1 Reagent Kit v1.5 (200 cycles; cat. no. 20028318; Illumina, Inc.) or NovaSeq 6000 S2 Reagent Kit v1.5 (200 cycles; cat. no. 20028315; Illumina, Inc.) were used. The loading concentration of the final library was 420 pM or 380 pM, and concentrations were measured using KAPA Library Quantification DNA Control Standard (KAPA Biosystems; Roche Diagnostics). The sequencing was performed by the NGS core facility at the Research Institute for Microbial Diseases of Osaka University.

Mutated serine and arginine rich splicing factor 2 (SRSF2) in myelodysplastic syndrome (MDS) compared with healthy controls for the percentage of exon 3. Mutations in genes encoding RNA splicing factors have been found in myeloid tumors, such as MDS (16,17), chronic myelomonocytic leukemia (17) and secondary acute myeloid leukemia (18,19), lymphoid tumors, such as chronic lymphocytic leukemia (19), and solid tumors, such as breast (20), lung (21) and pancreatic (22) cancer at high frequency. The present study focused on the splicing defects in MDS. Given that splicing factor 3B subunit 1, SRSF2 and U2 small nuclear RNA auxiliary factor 1 are the most frequently mutated splicing factor genes in MDS (16), and since the splicing mechanism of SRP9 in pancreatic cancer remains to be fully investigated, the present study focused on the altered control of the SRP9 splicing mechanism in a well-characterized hematopoietic malignancy as a disease model. Using the state-of-the-art supercomputer system at the National Institute of Genetics (Japan), which provides services equipped with large-scale clustered and memory-sharing computers (https://sc.ddbj.nig.ac.jp/en/), a comprehensive analysis was performed to determine the effects of mutated SRSF2 on pre-mRNA splicing in splicing factor mutant MDS stem/progenitor cells and erythroid/myeloma progenitor cells.

Using the Gene Expression Omnibus database (https://www.ncbi.nlm.nih.gov/geo/; accession no. GSE114922), 15 samples from healthy individuals and 15 samples from patients with MDS (SRSF2 mutation) were collected. Data (fastq files) were downloaded and the fastq files were mapped using Hisat2. Then, they were sorted, creating bam files (Fig. S6A and B). The sorted bam files were then checked for SRP9 expression using Integrative Genomics Viewer (IGV; mapping results visualization software; https://igv.org), and the percentage of exon 3 or v1 was compared between the healthy and SRSF2-mutant groups (Fig. S6C).

Statistical analysis. Data are presented as the mean and standard deviation or the median and range. The relationship between two groups was examined using the Mann-Whitney U and log rank tests. The relationship between nuclear staining rate and Ki-67 was examined by single regression analysis. For multi-group comparisons of three or more groups, the Kruskal-Wallis test and subsequent Dunn test were performed. Bonferroni correction was performed for Dunn test ($P<0.05/3$ were significant). Statistical analyses were performed using Statcel (version 4; OMS). $P<0.05$ was considered to indicate a statistically significant difference.

Results

Comparison of patient background and prognosis (RFS and OS) between two SRP9 expression groups. Patients were divided into two groups: Those with ≤50% of the total number of nuclei stained at the tumor site (n=14; Fig. 1A) and those with >50% staining (n=24; Fig. 1B). The patient background (Table I) and prognoses, such as RFS and OS, were compared between the two groups (Fig. 1C and D). The percentage of no lymphatic invasion (ly0) was significantly higher in the nuclear staining >50% group. However, no significant differences in the other parameters, including the tumor diameter and the prognostic nutritional index (PNI), which indicates the nutritional status of the patients, were observed between the two groups (Table I and Fig. S7). The group with nuclear staining >50% had a significantly better RFS ($P=0.037$; Fig. 1C), whereas OS was not significantly different between the two groups ($P=0.604$; Fig. 1D). These results showed that nuclear translocation of SRP9 contributed to patient prognosis (in terms of RFS), although no significant difference in OS was observed.

Relationship between Ki-67 and the nuclear staining rate. Immunohistochemistry with Ki-67 was performed on the same aforementioned cases to confirm whether the significant difference in RFS obtained in Fig. 1C was due to tumor proliferative capacity. For this, the correlation between Ki-67 and

Table I. Patient background.

Clinical characteristic	Nuclear staining ≤50%, n=14	Nuclear staining >50%, n=24	P-value
Age, years [range]	69.5 [50-84]	70.5 [51-87]	0.440
Female:male (% female)	6:8 (42.9)	5:19 (20.8)	0.266
Tumor site, Ph:Pb:Pt	9:4:1	10:7:7	0.455
Procedure classification, DP:PD (% DP)	5:9 (35.7)	14:10 (58.3)	0.202
pT[a] (%)			0.927
1	1 (7.1)	1 (4.2)	
2	0 (0.0)	1 (4.2)	
3	13 (92.9)	22 (91.7)	
4	0 (0.0)	0 (0.0)	
pN[a] (%)			0.145
0	4 (28.6)	9 (37.5)	
1	4 (28.6)	12 (50.0)	
2	6 (42.9)	3 (12.5)	
pStage[a] (%)			0.338
IA	1 (7.1)	1 (4.2)	
IB	0 (0.0)	1 (4.2)	
IIA	3 (21.4)	8 (33.3)	
IIB	9 (64.3)	14 (58.3)	
III	1 (7.1)	0 (0.0)	
pN^+:pN^- (% pN^+)	10:4 (71.4)	15:9 (62.5)	0.728
CA19-9, U/ml [range]	156 [0.4-1221]	181 [0.8-1839]	0.525
CEA, ng/ml [range]	3 [1-12]	3.5 [1-59]	0.446
DUPAN-2, U/ml [range]	265 [25-7700]	110 [25-1600]	0.069
HbA1c, % (NGSP) [range]	6.5 [5.9-8.2]	6.3 [5.4-8]	0.524
Prognostic nutritional index [range]	46.9 [37.8-54.0]	44.1 [38.0-54.9]	0.096
Tumor diameter, mm [range]	24.5 [8-43]	24 [10-120]	0.716
Histological type, muc:tub1:tub2:por	0:5:8:1	2:6:14:2	1.000
CH0:CH1 (% CH0)	9:5 (64.3)	20:4 (83.3)	0.245
DU0:DU1 (% DU0)	10:4 (71.4)	19:5 (79.2)	0.699
S0:S1 (% S0)	4:10 (28.6)	7:17 (29.2)	1.000
RP0:RP1 (% RP0)	5:9 (35.7)	8:16 (33.3)	1.000
A0:A1 (% A0)	13:1 (92.9)	18:6 (75.0)	0.227
PV0:PV1 (% PV0)	10:4 (71.4)	14:10 (58.3)	0.501
PL0:PL1 (% PL0)	14:0 (100.0)	24:0 (100.0)	1.000
INFb:INFc (% INFb)	12:2 (85.7)	23:1 (95.8)	0.542
ly0:ly1 (% ly0)	5:9 (35.7)	17:7 (70.8)	0.047[b]
v0:v1:v2:v3	9:4:1:0	15:3:4:2	0.610
ne0:ne1:ne2:ne3	0:10:3:1	4:9:9:2	0.805
OO0: OO1 (% OO0)	14:0 (100.0)	22:2 (91.7)	0.522
Postoperative chemotherapy (% received treatment)	13 (92.9)	16 (66.7)	0.115

[a]Defined using Unio Internationalis Contra Cancrum (8th edition) (38). [b]P<0.05 by Mann Whitney U Test. Ph, pancreatic head; Pb, pancreatic body; Pt, pancreatic tail; DP, distal pancreatectomy; PD, pancreaticoduodenectomy; pT, pathological tumor stage; pN, pathological lymph node stage; pStage, pathological stage; muc, mucinous; tub, tubular; por, poorly differentiated; CH, bile duct invasion (0, no invasion; 1, invasion; and the same thereafter); DU, duodenal invasion; S, anterior pancreatic tissue invasion; RP, posterior pancreatic tissue invasion; A, arterial invasion; PV, portal vein invasion; PL, extrapancreatic plexus invasion; ly, lymphatic invasion; v, vascular invasion (v0, no vascular invasion; v1, partial vascular invasion; v2, extensive vascular invasion; v3, very extensive vascular invasion); ne, intrapancreatic nerve invasion (ne0, no nerve invasion; ne1, mild nerve invasion; ne2, moderate nerve invasion; ne3, severe nerve invasion); OO, other organ invasion.

nuclear staining rate was examined. A representative image of immunohistochemical staining of pancreatic cancer with Ki-67 is presented (Fig. S1A). No clear trend was observed (R^2=0.007; P=0.622; Fig. S1B). The results therefore indicated

that the nuclear staining rate was associated with RFS but not with the proliferative capacity.

Immunocytochemistry to evaluate differences in nuclear translocation rates between pancreatic cancer lines cultured in normal and amino acid-deficient media. Representative images of SRP9 and nuclei immunocytochemically stained samples from the four groups [MTN (+) (Fig. S2A), M(-) (Fig. S2B), TN(-) (Fig. S2C), and MTN (-) (Fig. S2D)] are shown. MiaPaCa cells were cultured in regular medium [MTN(+)], M(-), TN(-), and MTN(-), and the nuclear translocation rates were compared using the equations expressed as S and R. The Kruskal-Wallis test was used to determine the difference in nuclear translocation rates of MiaPaCa cells cultured in M(-), TN(-), MTN(-) and MTN(+) media, as determined by the S and R equations, which showed significant differences ($P<0.0001$ for each; Fig. 2F and G). The nuclear transfer rates in the control MTN(+) medium were then compared with that in the other three media [MTN(+) vs. M(-), MTN(+) vs. TN(-), and MTN(+) vs. MTN(-)] using the Kruskal-Wallis test followed by the Dunn test. The nuclear translocation rate of MiaPaCa cells was significantly lower when cultured in M(-), TN(-) or MTN(-) media compared with the MTN(+) medium, for both the equations expressed as S (Fig. 2F) or R (Fig. 2G). These results indicated that amino acid deficiency suppressed nuclear translocation of SRP9.

PCR quantification of v1 and v2 when cells were cultured in amino acid-deficient medium. The PCR results showed that the bands were separated into v1 and v2 in the four medium groups (Fig. S3A). v1 was predicted to be 398 bp. However, it was shown that the band was 500 bp due to ~100 bp of some unexpected sequences. The ratio of v1 to v2 (v1/v2) of those cells cultured in M(-), TN(-), MTN(-) and MTN(+) media was quantified by measuring the band density following electrophoresis. No notable differences were observed among the four groups [M(-) vs. TN(-) vs. MTN(-) vs. MTN(+), 0.59 vs. 0.54 vs. 0.57 vs. 0.53); Fig. S3B]. The housekeeping gene, GAPDH, was also confirmed to be amplified by electrophoresis (Fig. S3C).

Evaluation of nuclear translocation of artificially constructed SRP9 isoforms. Transfection of plasmids containing the genes for v1 (Fig. 3D) and v2 (Fig. 3E) and the common parts of v1 and v2 (Fig. 3F) confirmed the nuclear translocation of v1 and v2, when compared with MOCK cells (Fig. 3C). This result indicated that the common parts of v1 and v2, exons 1 and 2, contain the coding regions important for nuclear translocation.

Functional evaluation of v1 and v2 using RIP sequencing. First, the genes and pathways that were upregulated/downregulated in the RIP1, RIP2, INPUT1 and INPUT2 samples were examined (Fig. 4A). Fig. 4F shows the heatmap for RIP1, RIP2, INPUT1 and INPUT2, and detailed heatmap data are shown in Table SI. The number of genes upregulated and downregulated in the RIP samples compared with the INPUT samples was 9,802 and 2,117, respectively (Table SI). In the volcano plot, genes related to tRNAs in mitochondria, such as MT-TV (log2 fold change=-15.63; $P=2.75x10^{-2}$), MT-TI (log2 fold change=-14.42; $P=2.75x10^{-2}$) and MT-TS2 (log2 fold change=-14.28; $P=2.75x10^{-2}$), were found to be downregulated in the RIP samples (Fig. 4G). The third largest fold change gene upregulated in the RIP samples was RN7SL327P (log2 fold change=8.14; $P=4.19x10^{-2}$), which is a mutant of RN7SL1 (Fig. 4G). The first and second largest fold changes were those whose gene symbols had not been identified.

Table II shows the enriched pathways related to the differentially expressed genes for RIP1 + RIP2 vs. INPUT1 + INPUT2. Next, RIP1, RIP2, INPUT1 and INPUT2 were clustered using the k-means algorithm (Fig. 4H), and Table III shows the pathways enriched in each cluster. Pathways involved in translation and protein synthesis, such as mitochondrial translational elongation, mitochondrial translational termination, translational termination, mitochondrial translation, cellular protein complex disassembly and protein-containing complex subunit organization, were classified. Table SII shows the detailed k-means data, and the pathways enriched in the Generally Applicable Gene-set Enrichment are shown in Table IV. Pathways involved in protein synthesis, such as ribonucleoprotein complex biogenesis, ribosome biogenesis and RNA splicing, were found to be downregulated in the RIP samples. GSEA was then used to analyze the gene expression data for RIP1 + RIP2 vs. INPUT1 + INPUT2, showing the three highest absolute values of normalized enrichment score (Fig. 4I). MYC, E2F and G2M checkpoints, which are pathways related to cancer progression, were found to be downregulated in the RIP samples. Furthermore, the GSEA of RIP1 vs. INPUT1 (Fig. 4J) and RIP2 vs. INPUT2 (Fig. 4K) showed downregulation of pathways related to cancer progression, although the ranking of the pathways varied. In GSEA comparing RIP1 vs. RIP2, the oxidative phosphorylation pathway was more downregulated in RIP1, whereas pathways related to the mitotic spindle and GM2 checkpoint were more downregulated in RIP2 (Fig. 4L). In RIP1 + RIP2 vs. INPUT1 + INPUT2, RIP1 vs. INPUT1, and RIP2 vs. INPUT2, the KRAS signaling DN (downregulated) pathway was the most upregulated pathway in the RIP samples (Fig. 4M). Details of the upregulated KRAS signaling DN pathways in RIP1 + RIP2 vs. INPUT1 + INPUT2 (Table SIII), RIP1 vs. INPUT1 (Table SIV), and RIP2 vs. INPUT2 (Table SV) are presented. The results demonstrated that the nuclear-translocated v1 and v2 downregulated genes and pathways are involved in protein translation and pathways associated with cancer progression.

In vitro tumor viability under amino acid depletion. The relationship between methionine and cancer development was investigated, as shown in Fig. S4A. Methionine deficiency suppressed tumor viability in Panc10.05, Caski and 293T cells (Fig. S4B-D). The results suggested that tumors were underdeveloped in a methionine-deficient environment.

RNA sequencing of tumors from mice fed diets excluding methionine/tryptophan/niacin. The relationship between amino acid deficiency and specific gene expression *in vivo* was examined (Fig. S5A). RNA sequencing of the tumor from a mouse (n=1) fed a diet devoid of methionine/tryptophan/niacin showed increased expression of RN7SL1, a non-coding RNA (Fig. S5B). During the experimental period, the maximum tumor volume was 144 mm^3 and the maximum tumor diameter

Table II. Enriched pathways in the differentially expressed genes for RIP1 + RIP2 vs. INPUT1 + INPUT2.

Direction	adj.P-value	Genes, n	Function in Gene Ontology
Downregulated	$7.1x10^{-46}$	229	RNA processing
	$2.1x10^{-43}$	211	MRNA metabolic process
	$2.2x10^{-36}$	465	Cellular component biogenesis
	$4.6x10^{-36}$	510	Organelle organization
	$7.7x10^{-35}$	473	Cellular localization
	$1.0x10^{-32}$	296	Cell cycle
	$2.6x10^{-32}$	137	MRNA processing
	$9.1x10^{-31}$	203	Mitotic cell cycle
	$2.2x10^{-30}$	122	RNA splicing
	$3.2x10^{-30}$	106	RNA splicing, via transesterification reactions
	$1.7x10^{-29}$	414	Macromolecule localization
	$2.9x10^{-29}$	104	RNA splicing, via transesterification reactions with bulged adenosine as nucleophile
	$2.9x10^{-29}$	104	MRNA splicing, via spliceosome
	$9.4x10^{-29}$	184	Protein localization to organelle
	$2.1x10^{-28}$	381	Establishment of localization in cell
Upregulated	$1.1x10^{-59}$	765	System process
	$2.3x10^{-42}$	526	Nervous system process
	$1.1x10^{-36}$	484	G protein-coupled receptor signaling pathway
	$1.6x10^{-30}$	364	Sensory perception
	$1.7x10^{-30}$	499	Ion transport
	$7.4x10^{-25}$	258	Regulation of ion transport
	$7.5x10^{-25}$	382	Cation transport
	$1.3x10^{-24}$	462	Biological adhesion
	$1.6x10^{-24}$	460	Cell adhesion
	$4.0x10^{-24}$	309	Metal ion transport
	$6.6x10^{-23}$	228	Detection of stimulus involved in sensory perception
	$2.8x10^{-22}$	365	Ion transmembrane transport
	$2.7x10^{-21}$	268	Detection of stimulus
	$4.4x10^{-21}$	282	Inorganic ion transmembrane transport
	$2.2x10^{-20}$	246	Chemical synaptic transmission

RIP, RNA immunoprecipitation (sample).

was 8 mm. The details of this RNA sequencing result are shown in Table SVI.

The aforementioned experiment was repeated and RNA sequencing of MTN(+) (n=1), M(-) (n=2), TN(-) (n=1) and MTN(-) (n=1) mice was also performed. It was found that mice without methionine or/and tryptophan or/and niacin [M(-), TN(-) and MTN (-) mice] tended to have elevated RN7SL1 levels compared with mice raised on a normal food diet [MTN(+)] (Fig. S5C). During the experimental period, the maximum tumor volume of the MTN(+) mouse was 100 mm^3 and the maximum tumor diameter was 8 mm; the maximum tumor volume of M(-) mouse 1 was 126 mm^3 and the maximum tumor diameter was 7 mm; the maximum tumor volume of M(-) mouse 2 was 144 mm^3 and the maximum tumor diameter was 8 mm; the maximum tumor volume of TN(-) mouse was 87.5 mm^3 and the maximum tumor diameter was 7 mm; and the MTN(-) mouse had a maximum tumor volume of 108 mm^3 and a maximum tumor diameter of 6 mm.

Mutated SRSF2 in MDS compared with healthy controls for the percentage of exon 3. In MDS, mutations in SRSF2 increased the percentage of exon 3 (v1) by an average of 4.2% compared with healthy controls (healthy vs. SRSF2 mutant, 14.9 vs. 19.1%) and by a median of 5.05% (healthy vs. SRSF2 mutant, P=0.002; Fig. S6C). This finding indicated that the splicing of SRP9 is affected by mutations in SRSF2.

Discussion

The present study focused on the localization of SRP9 and its variants. For this purpose, the 'Hoffman effect' (9-13) and the relationship between amino acid deficiency and cancer development is first discussed, then RN7SL1 (8,23,24), a non-coding

Table III. Enriched pathways for each cluster.

Cluster	adj.P-value	Genes, n	Function in Gene Ontology
A	$8.1x10^{-9}$	9	Mitochondrial translational elongation
	$8.1x10^{-9}$	9	Mitochondrial translational termination
	$2.3x10^{-8}$	9	Translational termination
	$1.5x10^{-7}$	9	Mitochondrial translation
	$2.2x10^{-7}$	9	Translational elongation
	$4.2x10^{-7}$	10	Cellular protein complex disassembly
	$4.2x10^{-7}$	26	Protein-containing complex subunit organization
	$4.2x10^{-7}$	9	Mitochondrial gene expression
	$1.0x10^{-6}$	9	Electron transport chain
	$1.3x10^{-6}$	11	Protein-containing complex disassembly
	$3.5x10^{-6}$	8	Oxidative phosphorylation
	$3.7x10^{-6}$	7	ATP synthesis coupled electron transport
	$8.9x10^{-6}$	7	Respiratory electron transport chain
	$1.9x10^{-5}$	8	Aerobic respiration
	$2.4x10^{-5}$	12	Cellular component disassembly
B	$6.9x10^{-3}$	2	L-phenylalanine metabolic process
	$6.9x10^{-3}$	2	Amino acid neurotransmitter reuptake
	$6.9x10^{-3}$	2	Lung-associated mesenchyme development
	$6.9x10^{-3}$	2	Erythrose 4-phosphate/phosphoenolpyruvate family amino acid metabolic process
D	$4.7x10^{-11}$	53	Sensory perception
	$8.2x10^{-11}$	39	Detection of stimulus involved in sensory perception
	$8.2x10^{-11}$	83	System process
	$1.7x10^{-10}$	36	Detection of chemical stimulus involved in sensory perception
	$3.5x10^{-10}$	37	Sensory perception of chemical stimulus
	$3.5x10^{-10}$	63	Nervous system process
	$3.5x10^{-10}$	33	Detection of chemical stimulus involved in sensory perception of smell
	$6.0x10^{-10}$	36	Detection of chemical stimulus
	$1.0x10^{-9}$	33	Sensory perception of smell
	$1.8x10^{-9}$	41	Detection of stimulus
	$5.4x10^{-6}$	51	G protein-coupled receptor signaling pathway
	$4.5x10^{-5}$	57	Locomotion
	$1.5x10^{-4}$	28	Chemotaxis
	$1.5x10^{-4}$	28	Taxis
	$2.4x10^{-4}$	29	Regulation of ion transport

RNA that binds to SRP9 and is upregulated *in vitro* under amino acid deficiency, is introduced.

A previous study involving animal experiments with rats has shown that, by depleting various amino acids in the diet, methionine deficiency inhibits tumor growth at the individual level and that methionine plays an important role in the development and progression of cancer (9). Methionine is an essential amino acid and is the codon that initiates protein translation from mRNA. Methionine is converted to SAM, which is required for nucleic acid synthesis in cancer (10). Tumors are underdeveloped in a methionine-deficient environment, which is known as the 'Hoffman effect' (9-13). A previous report has shown that tumor growth is suppressed in the absence of methionine, and methionine has recently been shown to be essential in cancer stem cells or 'tumor-initiating cells' (11). Additionally, methionine has been reported to influence tumor cell metabolism (12), histone patterns and T-cell immunity in the cancer microenvironment (13). Not only methionine, but also its upstream pathways have been reported to be involved in cancer immunity (14) (Fig. 2A). Tryptophan/niacin, which is located upstream of the methionine cycle, is metabolized to form nicotinamide, and MNAM is formed from SAM and nicotinamide via nicotinamide N-methyltransferase (NNMT) (14). NNMT and MNAM have been reported to participate in the mechanism of inhibition of the apoptosis signal-regulated kinase 1-p38 MAPK pathway, resulting in increased colon cancer cell resistance to 5-FU (25). NNMTs promote nicotinamide adenine dinucleotide depletion and epigenetic reprogramming, which have been implicated in the development of metabolic plasticity, circumvention of the major tumor suppressive process of cellular senescence, acquisition of stem cell properties, resistance to therapy and poor

Table IV. Enriched pathways for GAGE.

Direction	GAGE analysis: RIP vs. INPUT	Statistic	Gene, n	adj.P-value
Downregulated	Ribonucleoprotein complex biogenesis	-20.0362	466	$4.2x10^{-69}$
	Ribosome biogenesis	-17.4508	328	$2.3x10^{-51}$
	RNA splicing	-17.1448	446	$2.1x10^{-53}$
	NcRNA processing	-16.8357	425	$3.2x10^{-51}$
	RNA splicing, via transesterification reactions	-16.1232	353	$1.2x10^{-46}$
	RNA splicing, via transesterification reactions with bulged adenosine as nucleophile	-15.982	350	$5.1x10^{-46}$
	MRNA splicing, via spliceosome	-15.982	350	$5.1x10^{-46}$
	RRNA processing	-15.734	262	$9.5x10^{-42}$
	RRNA metabolic process	-15.4495	272	$3.5x10^{-41}$
	RNA catabolic process	-15.0928	418	$1.0x10^{-42}$
	MRNA catabolic process	-14.8794	376	$3.5x10^{-41}$
	Translational initiation	-14.2285	194	$3.0x10^{-33}$
	Proteasomal protein catabolic process	-13.9713	490	$5.9x10^{-38}$
	Regulation of cell cycle phase transition	-13.4307	499	$2.0x10^{-35}$
	Regulation of mRNA metabolic process	-13.2654	367	$1.2x10^{-33}$
	Proteasome-mediated ubiquitin-dependent protein catabolic process	-13.2598	435	$4.0x10^{-34}$
	Protein targeting	-13.1615	394	$1.7x10^{-33}$
	DNA replication	-13.0678	336	$2.0x10^{-32}$
	Regulation of mitotic cell cycle phase transition	-13.0076	413	$6.1x10^{-33}$
	Regulation of translation	-12.9471	404	$1.3x10^{-32}$
	Nuclear-transcribed mRNA catabolic process	-12.8684	209	$2.6x10^{-29}$
	Establishment of protein localization to membrane	-12.672	380	$2.7x10^{-31}$
	Regulation of cellular amide metabolic process	-12.5776	466	$2.2x10^{-31}$
	Viral gene expression	-12.4686	235	$1.5x10^{-28}$
	Mitotic nuclear division	-12.4212	340	$7.9x10^{-30}$
Upregulated	Detection of chemical stimulus involved in sensory perception	13.0713	392	$2.2x10^{-31}$
	Detection of chemical stimulus involved in sensory perception of smell	12.8671	352	$1.7x10^{-30}$
	Detection of stimulus involved in sensory perception	12.8423	455	$2.8x10^{-31}$
	Detection of chemical stimulus	12.5666	426	$4.4x10^{-30}$
	Sensory perception of smell	12.3795	376	$6.5x10^{-29}$

GAGE, Generally Applicable Gene-set Enrichment; RIP, RNA immunoprecipitation (sample).

clinical outcomes (26). Furthermore, MNAM synthesized in this methionine cycle has been reported to suppress T cells and promote cancer (15).

Therefore, in the present study, the HT-29 human colon cancer cell line cultured in a normal medium with all nutrients was implanted into NOD SCID mice, which were maintained for 2 weeks on a diet without methionine/tryptophan/niacin. The tumors of these mice were then removed and RNA sequencing was performed. A marked increase in the expression of RN7SL1, a non-coding RNA, was observed in the tumor. The RN7SL1 variant termed 'RN7SL327P' was also upregulated in SRP9 v1 and v2 transfected cells subjected to RIP sequencing. A previous study at another institution found that co-culturing breast cancer cells with stromal fibroblasts resulted in the stromal fibroblasts releasing RN7SL1 contained in exosomes, which were transported to the cancer cells, resulting in tumor growth (8). RN7SL1 has also been reported to have a reliable clinical performance for hepatocellular carcinoma diagnosis and prognosis (23). It has been reported that CAR-T cells transduce RN7SL1 into extracellular vesicles and activate RIG-I, and that transfection of immune-competent mice with tumor cells overexpressing RN7SL1 leads to increased activation of RIG-I/MDA5 by immune cells and improved survival rather than tumor growth (24). Therefore, this is still a highly controversial topic.

Previously, we attempted to localize RN7SL1. However, single-cell analysis is difficult due to RN7SL1 being a non-coding RNA and not having a 3′-UTR poly A tail sequence. Furthermore, *in situ* hybridization is difficult as RN7SL1 contains an Alu domain. Therefore, the present study focused on proteins that are thought to bind to RN7SL1, which is divided into Alu and S domains, with the Alu domain binding

to SRP9/14 and the S domain binding to SRP19/54/68/72 (1). Of these, high SRP9 expression tends to be related to a worse OS in patients with pancreatic cancer, according to the Human Protein Atlas database (https://www.proteinatlas.org/ENSG00000143742-SRP9/pathology/pancreatic+cancer). The group with high SRP72 expression had a significantly worse OS (https://www.proteinatlas.org/ENSG00000174780-SRP72/pathology/pancreatic+cancer). Additionally, no significant differences regarding the other SRP families [SRP9/14 (https://www.proteinatlas.org/ENSG00000140319-SRP14/pathology/pancreatic+cancer)/19 (https://www.proteinatlas.org/ENSG00000153037-SRP19/pathology/pancreatic+cancer)/54 (https://www.proteinatlas.org/ENSG00000100883-SRP54/pathology/pancreatic+cancer)/68 (https://www.proteinatlas.org/ENSG00000167881-SRP68/pathology/pancreatic+cancer)] were observed between the two expression groups. Regarding the relationship between SRP9 and tumors, a previous report on colorectal cancer reported that SRP9 acts in a tumor proliferative manner (4), and a report on breast cancer showed that when tumor tissue and surrounding normal breast tissue were collected from patients undergoing breast cancer surgery, SRP9 expression was higher in the tumor cells (2).

Although the GeneCards database (https://www.genecards.org/cgi-bin/carddisp.pl?gene=SRP9) shows that SRP9 is predominantly found in the cytoplasm, its localization in the tumor microenvironment has not yet, to the best of our knowledge, been clarified. The present study examined SRP9 in detail and its relationship with patient prognosis using clinical data. Notably, in pancreatic cancer, the group with >50% nuclear staining at the tumor site had a significantly better RFS than the group with <50%. Next, cell immunostaining was performed to determine the nuclear translocation rate, referring to previous reports of DsRed incorporated into yeast plasmid vectors and overlapping with DAPI (27) and a subsequent study examining nuclear β-catenin translocation (28). Furthermore, the present study confirmed that the nuclear translocation rate of SRP9 was significantly reduced by methionine/niacin/tryptophan deficiency. When integrating these results with the immunohistochemistry results, it would appear that RFS is poor under a low nuclear transfer rate, that is, amino acid deficiency, which may not be consistent with the traditionally accepted Hoffman effect. However, *in vitro* experiments and experiments using human specimens, in which various factors overlap, can produce opposite results. In other words, it is true that nuclear translocation of SRP9 protein is closely related to the prognosis of patients with pancreatic cancer, but this cannot be explained simply by the involvement of methionine alone, suggesting that multiple factors are involved in the phenomenon of nuclear translocation of SRP9 protein in pancreatic cancer cells. Indeed, a cohort study conducted in Sweden suggested that higher methionine intake may reduce the risk of pancreatic cancer (29). In another meta-analysis, a non-significant borderline risk reduction (risk ratio=0.81; 95% confidence interval, 0.62-1.01) was found in the overall population for methionine intake and risk of developing pancreatic cancer, but no association was observed in any subgroup by study design, region or number of cases (30). The Hoffman effect is well known and important, but it should be noted that it is but one aspect of the *in vitro* story. For example, hypothetically, cancer cells themselves could deplete methionine and reduce biological malignant traits such as cell proliferation, but at the individual patient level, methionine depletion would be expected to be involved not only in immune responses but also in sarcopenic responses, such as glucose metabolism and even stromal and muscle metabolism. In addition, with regards to the nuclear translocation of SRP9, while amino acids such as methionine are certainly involved, multiple other factors are involved in the nuclear translocation phenomenon. Although it may be shortsighted, in the present study, the PNI was also measured as a simple preoperative nutritional indicator using lymphocyte and albumin levels for patients with pancreatic cancer who underwent immunohistochemistry, and no significant difference was found between the two groups, nuclear staining ≤50% and nuclear staining >50%. These results indicated that the prognostic change in the nuclear translocation rate was not simply due to the nutritional index of the patient but to functional changes in SRP9 molecules that have translocated to the nucleus.

Subsequently, the present study focused on two variants of SRP9, v1 and v2. The results indicated that there were no notable splicing effects by depleting methionine/niacin/tryptophan, as aforementioned. Transfection of plasmids incorporating genes of v1 and v2 and the common parts of v1 and v2 into a number of pancreatic cancer cell lines confirmed the nuclear translocation of SRP9. This suggested that the common parts of v1 and v2, exon1 and exon2, contained coding regions important for nuclear translocation. In addition, there appeared to be slightly less SRP9 staining in v1 and the common parts of v1 and v2, which may be due to v2 being more dominant than v1.

Since both v1 and v2 were found to be nuclear translocating molecules, RIP sequencing was subsequently performed in the present study using cells transfected with either variant (Fig. 4A). The results showed that genes and pathways involved in protein translation were downregulated by nuclear migration in both RIP1 and RIP2. A previous report showed that SRP complexes, including RN7SL1, bind to ribosomes and carry them to translocons in the endoplasmic reticulum membrane to transport synthesized proteins to target cells (31), and that this function is inhibited by translocation into the nucleus. Therefore, in the present study, amino acid deficiency may have suppressed nuclear translocation of SRP9 in an attempt to promote translation and may have also increased RN7SL1 expression, which binds to SRP9 and is responsible for translation, by a feedback mechanism. Additionally, both RIP1 and RIP2 downregulated pathways were involved in cancer progression, and this finding was consistent with the SRP9 immunohistochemistry results, in which the nuclear staining >50% group had significantly better RFS than the nuclear staining ≤50% group. Consistent with the GSEA analysis, c-Myc (32), E2F-1 (33), G2M checkpoint (34), oxidative phosphorylation (35), unfolded protein response (36) and KRAS mutation (37) have been reported to be associated with pathways in pancreatic cancer development.

There are two limitations to the present study. First, the immunohistochemistry of pancreatic cancer in Fig. 1, which was the origin of the study, was limited to cases that had not been treated preoperatively, in favor of ease of pathological evaluation. Future studies are needed to determine the diagnostic value of SRP9 translocation in cases treated with preoperative chemotherapy or preoperative radiation chemotherapy. Second,

the present study showed that SRP9 nuclear translocation is suppressed under amino acid deficiency, and that the coding region important for nuclear translocation may be located in exons 1 and 2, the common part of v1 and v2, but the detailed mechanism of nuclear translocation remains to be elucidated.

In conclusion, in the present study, immunohistochemical staining of SRP9 in pancreatic cancer specimens, a protein that binds to RN7SL1, showed that the RFS of patients was significantly improved when the nuclear translocation rate was >50% at the tumor site. In addition, amino acid (methionine/niacin/tryptophan) deficiency reduced the nuclear translocation rate. There are two variants of SRP9, v1 and v2. However, splicing was not significantly affected by amino acid deletion, and the common parts of v1 and v2, exons 1 and 2, contain coding regions important for nuclear translocation. Additionally, the RIP sequencing results obtained following nuclear translocation of the v1 and v2 plasmids showed that both plasmids downregulated the genes/pathways related to protein translation and the pathways involved in cancer progression. However, further studies on the mechanism of SRP9 nuclear translocation and its detailed function are needed.

Acknowledgements

Not applicable.

Funding

This work was supported in part by a Grant-in-Aid for Scientific Research from the Ministry of Education, Culture, Sports, Science and Technology [grant nos. 17cm0106414h0002, JP21lm0203007, 18KK0251, 19K22658, 20H00541, 21K19526, 22H03146, 22K19559, 23K19505 and 16H06279 (PAGS)]. Partial support was also offered by the Mitsubishi Foundation (grant no. 2021-48) to HI.

Availability of data and materials

The RIP and RNA sequencing data generated in the present study may be found in the Gene Expression Omnibus repository under accession numbers GSE246628, GSE256049, and GSE256061. All other data generated in the present study may be requested from the corresponding author.

Authors' contributions

HS, SM, KS, SK, KK, SU, KO, TS, YD, HE, TH and HI made substantial contributions to conception and design. HS, SM, KS, SK, KK, YTs, YA, YS, YI, DY, YTo, TN, HT, DM, KO, TS, YD, HE, TH and HI acquired the data. HS, SM, KS, SK, KK, YTs, YI, DY, YTo, TN, HT, DM, YD, HE, TH and HI analyzed and interpreted the data. HS, SM, TH and HI confirmed the authenticity of all the raw data. HS, SM, KK, YTs, YA, YS, DM, KO, TH and HI performed the research. HS, SM, KK, TH and HI evaluated the percentage of nuclear staining in the immunohistochemistry. HS, SM, SU, KO, TH and HI wrote the manuscript. HS, SM, KS, SK, YI, DY, YTo, TN, HT, DM, SU, KO, TS, YD, HE, TH and HI revised the manuscript. KS, SK, SU, TS, YD, HE, TH and HI supervised the work. All authors read and approved the final version of the manuscript.

Ethics approval and consent to participate

This study was approved by the Research Ethics Committee of Osaka University (Osaka, Japan; approval no. 23158). Informed consent was obtained from all subjects involved in the study.

Patient consent for publication

Written informed consent has been obtained from the patients to publish this paper.

Competing interests

Partial institutional endowments were received from Hirotsu Bio Science, Inc. (Tokyo, Japan); Kinshu-kai Medical Corporation (Osaka, Japan); Kyowa-kai Medical Corporation (Osaka, Japan); IDEA Consultants, Inc. (Tokyo, Japan); and Unitech Co., Ltd. (Chiba, Japan). KO is an employee of IDEA Consultants, Inc. The remaining authors declare that they have no competing interests.

References

1. Kellogg MK, Tikhonova EB and Karamyshev AL: Signal recognition particle in human diseases. Front Genet 13: 898083, 2022.
2. Erdogan G, Trabulus DC, Talu CK and Guven M: Investigation of SRP9 protein expression in breast cancer. Mol Biol Rep 49: 531-537, 2022.
3. Rho JH, Qin S, Wang JY and Roehrl MH: Proteomic expression analysis of surgical human colorectal cancer tissues: Up-regulation of PSB7, PRDX1, and SRP9 and hypoxic adaptation in cancer. J Proteome Res 7: 2959-2972, 2008.
4. Zhang M, Peng Y, Yang Z, Zhang H, Xu C, Liu L, Zhao Q, Wu J, Wang H and Liu J: DAB2IP down-regulates HSP90AA1 to inhibit the malignant biological behaviors of colorectal cancer. BMC Cancer 22: 561, 2022.
5. Hessel EV, de Wit M, Wolterink-Donselaar IG, Karst H, de Graaff E, van Lith HA, de Bruijn E, de Sonnaville S, Verbeek NE, Lindhout D, *et al*: Identification of Srp9 as a febrile seizure susceptibility gene. Ann Clin Transl Neurol 1: 239-250, 2014.
6. Bovia F, Fornallaz M, Leffers H and Strub K: The SRP9/14 subunit of the signal recognition particle (SRP) is present in more than 20-fold excess over SRP in primate cells and exists primarily free but also in complex with small cytoplasmic Alu RNAs. Mol Biol Cell 6: 471-484, 1995.
7. Berger A, Ivanova E, Gareau C, Scherrer A, Mazroui R and Strub K: Direct binding of the Alu binding protein dimer SRP9/14 to 40S ribosomal subunits promotes stress granule formation and is regulated by Alu RNA. Nucleic Acids Res 42: 11203-11217, 2014.
8. Nabet BY, Qiu Y, Shabason JE, Wu TJ, Yoon T, Kim BC, Benci JL, DeMichele AM, Tchou J, Marcotrigiano J and Minn AJ: Exosome RNA unshielding couples stromal activation to pattern recognition receptor signaling in cancer. Cell 170: 352-366 e13, 2017.
9. Sugimura T, Birnbaum SM, Winitz M and Greenstein JP: Quantitative nutritional studies with water-soluble, chemically defined diets. VIII. The forced feeding of diets each lacking in one essential amino acid. Arch Biochem Biophys 81: 448-455, 1959.
10. Kaiser P: Methionine dependence of cancer. Biomolecules 10: 568, 2020.
11. Wang Z, Yip LY, Lee JHJ, Wu Z, Chew HY, Chong PKW, Teo CC, Ang HY, Peh KLE, Yuan J, *et al*: Methionine is a metabolic dependency of tumor-initiating cells. Nat Med 25: 825-837, 2019.
12. Gao X, Sanderson SM, Dai Z, Reid MA, Cooper DE, Lu M, Richie JP Jr, Ciccarella A, Calcagnotto A, Mikhael PG, *et al*: Dietary methionine influences therapy in mouse cancer models and alters human metabolism. Nature 572: 397-401, 2019.

13. Bian Y, Li W, Kremer DM, Sajjakulnukit P, Li S, Crespo J, Nwosu ZC, Zhang L, Czerwonka A, Pawłowska A, *et al*: Cancer SLC43A2 alters T cell methionine metabolism and histone methylation. Nature 585: 277-282, 2020.
14. Tatekawa S, Ofusa K, Chijimatsu R, Vecchione A, Tamari K, Ogawa K and Ishii H: Methylosystem for cancer sieging strategy. Cancers (Basel) 13: 5088, 2021.
15. Kilgour MK, MacPherson S, Zacharias LG, Ellis AE, Sheldon RD, Liu EY, Keyes S, Pauly B, Carleton G, Allard B, *et al*: 1-Methylnicotinamide is an immune regulatory metabolite in human ovarian cancer. Sci Adv 7: eabe1174, 2021.
16. Pellagatti A, Armstrong RN, Steeples V, Sharma E, Repapi E, Singh S, Sanchi A, Radujkovic A, Horn P, Dolatshad H, *et al*: Impact of spliceosome mutations on RNA splicing in myelodysplasia: Dysregulated genes/pathways and clinical associations. Blood 132: 1225-1240, 2018.
17. Figg JW, Barajas JM and Obeng EA: Therapeutic approaches targeting splicing factor mutations in myelodysplastic syndromes and acute myeloid leukemia. Curr Opin Hematol 28: 73-79, 2021.
18. Wang E, Pineda JMB, Kim WJ, Chen S, Bourcier J, Stahl M, Hogg SJ, Bewersdorf JP, Han C, Singer ME, *et al*: Modulation of RNA splicing enhances response to BCL2 inhibition in leukemia. Cancer Cell 41: 164-180 e8, 2023.
19. Rahman MA, Lin KT, Bradley RK, Abdel-Wahab O and Krainer AR: Recurrent SRSF2 mutations in MDS affect both splicing and NMD. Genes Dev 34: 413-427, 2020.
20. Yang Q, Zhao J, Zhang W, Chen D and Wang Y: Aberrant alternative splicing in breast cancer. J Mol Cell Biol 11: 920-929, 2019.
21. Nanjo S, Wu W, Karachaliou N, Blakely CM, Suzuki J, Chou YT, Ali SM, Kerr DL, Olivas VR, Shue J, *et al*: Deficiency of the splicing factor RBM10 limits EGFR inhibitor response in EGFR-mutant lung cancer. J Clin Invest 132: e145099, 2022.
22. Wan L, Lin KT, Rahman MA, Ishigami Y, Wang Z, Jensen MA, Wilkinson JE, Park Y, Tuveson DA and Krainer AR: Splicing Factor SRSF1 promotes pancreatitis and KRASG12D-mediated pancreatic cancer. Cancer Discov 13: 1678-1695, 2023.
23. Tan C, Cao J, Chen L, Xi X, Wang S, Zhu Y, Yang L, Ma L, Wang D, Yin J, *et al*: Noncoding RNAs serve as diagnosis and prognosis biomarkers for hepatocellular carcinoma. Clin Chem 65: 905-915, 2019.
24. Johnson LR, Lee DY, Eacret JS, Ye D, June CH and Minn AJ: The immunostimulatory RNA RN7SL1 enables CAR-T cells to enhance autonomous and endogenous immune function. Cell 184: 4981-4995 e14, 2021.
25. Xie X, Liu H, Wang Y, Zhou Y, Yu H, Li G, Ruan Z, Li F, Wang X and Zhang J: Nicotinamide N-methyltransferase enhances resistance to 5-fluorouracil in colorectal cancer cells through inhibition of the ASK1-p38 MAPK pathway. Oncotarget 7: 45837-45848, 2016.
26. Novak Kujundzic R, Prpic M, Dakovic N, Dabelić N, Tomljanović M, Mojzeš A, Fröbe A and Trošelj KG: Nicotinamide N-Methyltransferase in acquisition of stem cell properties and therapy resistance in cancer. Int J Mol Sci 22: 5681, 2021.
27. Rodrigues F, van Hemert M, Steensma HY, Corte-Real M and Leao C: Red fluorescent protein (DsRed) as a reporter in Saccharomyces cerevisiae. J Bacteriol 183: 3791-3794, 2001.
28. Kimura A, Toda Y, Matsumoto Y, Yamamoto H, Yahiro K, Shimada E, Kanahori M, Oyama R, Fukushima S, Nakagawa M, *et al*: Nuclear β-catenin translocation plays a key role in osteoblast differentiation of giant cell tumor of bone. Sci Rep 12: 13438, 2022.
29. Larsson SC, Giovannucci E and Wolk A: Methionine and vitamin B6 intake and risk of pancreatic cancer: A prospective study of Swedish women and men. Gastroenterology 132: 113-118, 2007.
30. Wei DH and Mao QQ: Vitamin B6, vitamin B12 and methionine and risk of pancreatic cancer: A meta-analysis. Nutr J 19: 111, 2020.
31. Kellogg MK, Miller SC, Tikhonova EB and Karamyshev AL: SRPassing Co-translational Targeting: The role of the signal recognition particle in protein targeting and mRNA protection. Int J Mol Sci 22: 6284, 2021.
32. Ala M: Target c-Myc to treat pancreatic cancer. Cancer Biol Ther 23: 34-50, 2022.
33. Peng YP, Zhu Y, Yin LD, Zhang JJ, Wei JS, Liu X, Liu XC, Gao WT, Jiang KR and Miao Y: PEG10 overexpression induced by E2F-1 promotes cell proliferation, migration, and invasion in pancreatic cancer. J Exp Clin Cancer Res 36: 30, 2017.
34. Oshi M, Patel A, Le L, Tokumaru Y, Yan L, Matsuyama R, Endo I and Takabe K: G2M checkpoint pathway alone is associated with drug response and survival among cell proliferation-related pathways in pancreatic cancer. Am J Cancer Res 11: 3070-3084, 2021.
35. Ashton TM, McKenna WG, Kunz-Schughart LA and Higgins GS: Oxidative phosphorylation as an emerging target in cancer therapy. Clin Cancer Res 24: 2482-2490, 2018.
36. Long D, Chen K, Yang Y and Tian X: Unfolded protein response activated by endoplasmic reticulum stress in pancreatic cancer: Potential therapeutical target. Front Biosci (Landmark Ed) 26: 1689-1696, 2021.
37. Luo J: KRAS mutation in pancreatic cancer. Semin Oncol 48: 10-18, 2021.
38. Brierley J, Gospodarowicz MK and Wittekind C: TNM Classification of Malignant Tumours. Wiley Blackwell, Hoboken, NJ, 2017.